FINAL REPORT

LAWRENCE LIVERMORE LABORATORY

PURCHASE ORDER NO. 7830209 DATED 03-01-72
WITH CHANGE ORDERS
NO. 1 ISSUED 06-27-72
and NO. 2 ISSUED 01-05-73

SUBMITTED BY

DR. A. L. GARDNER
DEPARTMENT OF PHYSICS AND ASTRONOMY
BRIGHAM YOUNG UNIVERSITY
PROVO, UTAH 84601

MAY 15, 1973

PREFACE

by

Andrew L. Gardner

The study required by this purchase order was carried out under my technical direction. A graduate student, Kenneth W. Struve, worked 300 hours of paid time on this study and his unpublished masters thesis in the ensuing pages covers the technical aspects of this final report which is required by the purchase order.

Although the study is not an exhaustive one, it gives meaningful information regarding a proposed measurement of the spatial electron distribution in the Baseball II system. Such a measurement still appears to be feasible, but now on firmer ground, and a suitable circular window is now available for such a measurement.

All who have been involved in the project at Brigham Young University appreciate the complete cooperation which was extended by L.L.L. and its employees in all joint aspects of the undertaking.

A STUDY OF THE TECHNIQUE OF UTILIZING A MICROWAVE FABRY-PEROT RESONATOR TO OBTAIN SPATIAL ELECTRON DENSITY DISTRIBUTIONS IN A MINIMUM-B PLASMA

Kenneth W. Struve

Department of Physics and Astronomy

M. S. Degree, April 1973

ABSTRACT

Near electron cyclotron resonance the spatial electron distribution in the direction of the confining magnetic field of some minimum-B, low β, plasmas can be measured with a confocal microwave Fabry-Perot resonator aligned along the direction of the confining field. The dielectric constant for the two circular polarizations varies as $(1 \pm \omega_b/\omega)^{-1}$, which factors can be determined by utilizing the knowledge of the axial variation of the confining magnetic field. The plasma is treated as a number of uniform slabs perpendicular to the resonator axis for which average density values can be determined by frequency shift measurements. The number of intervals is limited by the maximum number of frequency shifts observable.

A broadband tunable, microwave vacuum window suitable for use with circularly polarized waves was designed, tested and built for the 18 to 26.5 Ghz range. It was found to have a VSWR of 1.1 in the center of the range, and less than 2.2 at the extremes for a fixed setting at midrange. Coupling microwave power to and from the resonator is also investigated.

COMMITTEE APPROVAL:

Andrew L. Gardner, Committee Chairman

Vern C. Rogers, Committee Member

B. Kent Harrison, Department Chairman

A STUDY OF THE TECHNIQUE OF UTILIZING A MICROWAVE FABRY-PEROT RESONATOR TO OBTAIN SPATIAL ELECTRON DENSITY DISTRIBUTIONS IN A MINIMUM-B PLASMA

A Thesis

Presented to the

Department of Physics & Astronomy

Brigham Young University

In Partial Fulfillment

of the Requirements for the Degree

Master of Science

by

Kenneth W. Struve

April 1973

This thesis, by Kenneth W. Struve, is accepted in its present form by the Department of Physics and Astronomy of Brigham Young University as satisfying the thesis requirement for the degree of Master of Science.

Andrew L. Gardner, Committee Chairman

Vern C. Rogers, Committee Member

29 March 1973
Date

B. Kent Harrison, Department Chairman

Typed by: Sheri Pew

ACKNOWLEDGEMENTS

The author wishes to acknowledge the assistance of Dr. A. L. Gardner, of the Department of Physics and Astronomy, in helping with the design of the experiment and of the microwave vacuum window, and the machinist, Mr. Herbert Kirchhoff for his construction of the window and waveguide transitions, and Mr. Gene Meeks for his help in design and testing of the vacuum characteristics of the window.

This research has been partially supported by the Lawrence Livermore Laboratory of the University of California with Purchase Order No. 7830209 under AEC Contract No. W-7405-ENG-48.

The author would also like to thank his wife, Susan, for her patient understanding and encouragement.

TABLE OF CONTENTS

Page

LIST OF FIGURES

Figure | Page

I. INTRODUCTION

Since the first hydrogen bomb was exploded in 1952, many people have been interested in controlling thermonuclear reactions for peaceful power production. It has been estimated that the energy represented by the amount of deuterium in the oceans could last the world one billion years at a rate of over one hundred times our present rate of power consumption.[1] Furthermore, fusion power is clean and safe, yielding only one radioactive isotope, tritium, whose half-life is twelve and one-half years. This is much shorter than the half-lives of many of the waste products of fission reactors. But if the fusion "burn" is complete, this also disappears.

The major problems in controlling fusion reactions are that of building a "bottle" capable of controlling a plasma at thermonuclear temperatures, and of heating the plasma to fusion temperatures. A plasma is here taken to be a hot gas in which the electrons are all or partially stripped away from each atomic nucleus. Presently much work is being done on magnetic mirror systems and closed toroidal magnetic configurations.

In dealing with such high temperatures, measurements of the state of the plasma become very difficult. Heald and Wharton[2] suggest nine quantities which are of particular interest. These are: electron density distributions, electron temperature, ion density distributions, ion temperature, neutral atom density, plasma wave velocities, plasma instabilities, plasma sheath regions, and impurities. Most of these

quantities are measured with electromagnetic waves, typically radio waves and microwaves.

Heald and Wharton further list a number of ways to measure electron densities. These are given in Table 1 along with their ranges of usefulness. The use of the microwave interferometer has proven to be a very reliable technique. It measures densities in the range of 10^9 to 10^{14} electrons/cm^3.

In the Michelson interferometer a microwave signal is split, one wave being sent through the plasma and the other being used to calibrate the phase-shift of the transmitted wave. The magnitude of the phase-shift then gives integrated values of the electron density distribution along the beam path.

THE FABRY-PEROT INTERFEROMETER

In the microwave Fabry-Perot interferometer, which is also called an open resonator, a signal is allowed to reflect back and forth between two mirrors. If a plasma is introduced between the two mirrors, the resonant frequencies of the interferometer are shifted, and the Q's of the resonances are reduced. Measurements of the shift and the change in the Q then provide information about the electron distribution and collision frequency. The remainder of this thesis will be devoted to the application of the Fabry-Perot interferometer to the study of spatial electron density distributions.

The microwave Fabry-Perot interferometer usually consists of spherical reflectors separated a distance equal either to the reflector radius or diameter. The former is called the confocal resonator, the latter the focused or spherical resonator. Plane or cylindrical

Table 1

Methods of Electron Density and Distribution Measurements

Method	Min. Density ($electrons/cm^3$)	Max. Density ($electrons/cm^3$)	Restrictions
Microwave Interferometer	10^{10}[a]	10^{14}	
Microwave Cavity Perturbation	10^{8}	10^{12}	
Rf-conductivity Probes	10^{8}	10^{15}	For high collision rates
Microwave Scattering	10^{12}	10^{14}	Sensitive to instabilities
Optical Interferometer	10^{14}	10^{19}	
Optical Faraday Rotation	10^{16}	--	For 10,000 Gauss
Optical Spectroscopic Intensities	10^{13}	--	Equilibrium plasmas
Optical Scattering	10^{14}	10^{19}	
Optical Balmer Series Limit	10^{13}	10^{15}	
Particle Collectors	--	--	$10^{-6} < J_e < 1$ amp/cm^2; yields product qn_ev
Electron or Ion Beam Scattering	--	--	Sensitive to potential fluctuations

[a]More recent experiments have dropped this lower limit down to 10^9 and, in some instances, 10^8 electrons/cm^3.

mirrors may also be used, although the diffraction losses for these are much greater, resulting in a lower Q. The Q of the Fabry-Perot interferometer varies typically from 10,000 to 100,000, thus making it very sensitive to small perturbations in the dielectric constant between the mirrors.

The Fabry-Perot interferometer differs from a closed microwave cavity in that only the $TEM_{\ell pq}$ modes are propagated and no TE or TM modes exist. The integers ℓ and p represent the transverse mode numbers, and q represents the longitudinal mode number. Since the ℓ, $p \neq 0$ modes have higher diffraction losses, one need only consider the TEM_{00q} modes. Also, the higher order ℓ, p modes are degenerate. This makes the spectrum of resonance peaks very clean and easy to analyze. The condition for resonance[3] in both configurations is:

$$\frac{4b}{\lambda} = q + 2p + \ell + 1 \qquad (1)$$

where b is the radius of the reflectors and λ is the wavelength.

The focused and the confocal resonator differ significantly in their difficulty of alignment. The alignment of the confocal mirrors is almost trivial whereas the alignment of the focused resonator is very critical. The chief advantage of the focused resonator is that it gives the highest possible degree of field concentration at the center of the resonator thereby permitting better spatial resolution.[4] In most applications this advantage is sacrificed to utilize the confocal resonator's superior alignment properties.

Many people have investigated the Fabry-Perot resonator. Boyd and Gordon[5] first investigated a confocal spherical resonator with square boundaries for possible application to the MASER. Later, Boyd

and Kogelnik[6] discussed spherical mirrors with rectangular boundaries, as well as perturbations. Goubau and Schwering[7] investigated the spherical resonator with round mirrors in handling the mathematics of the Beam Waveguide. Primich and Hayami[8] first discussed the application of the Fabry-Perot resonator to plasma diagnostics. Chaffin[3] and Chaffin and Beyer[9,10] did a very comprehensive study of the plasma diagnostics of the Fabry-Perot resonator and compiled past results. Many others have also contributed, especially in the context of optical lasers.[11-17]

More recently Eaves, Twardeck, and Morin[18] investigated isotopic plasmas using the lower order modes of a Fabry-Perot resonator to give spatial electron density distributions. In 1971, Gardner[19] suggested using the spatial variation of a confining magnetic field of a minimum-B plasma such as that of the "Baseball II" to obtain information about the spatial electron distribution. The Eaves, Twardeck, and Morin approach utilizes the electric field configuration in much the same way as with a closed cavity to obtain the distribution, whereas the Gardner approach is to operate the resonator near the cyclotron resonance frequency to obtain a spatial sensitivity to the plasma. Gardner's approach will here be examined.

THE PROBLEM

This thesis will explore the feasibility of using the microwave Fabry-Perot interferometer to measure the spatial distribution of electrons in a minimum-B plasma using the spatial variation of the confining magnetic field along the interferometer axis. This involves a theoretical investigation of the diagnostic capabilities.

A second portion of the work is experimental in nature. This partially involves development and testing of a microwave window. This window is needed to allow transmission of circularly polarized waves through the vacuum container wall to permit observation of frequency shifts in these waves. A second part is the determination of a method to couple microwave power into and out of the resonator, which may be used at liquid helium temperatures, without conducting much heat through a waveguide structure.

OUTLINE OF THE DISCUSSION

The analysis will be discussed in terms of the "Baseball II" system at the Lawrence Livermore Laboratory. The "Baseball II" device derives its name from the configuration of the windings on its superconducting magnet, being shaped like the seam on a baseball. (See Figure 1) The Fabry-Perot resonator consists of two confocal spherical reflectors with rectangular boundaries turned 90° to each other and fitting between the poles of the magnet such that the propagation of the microwaves is along the axis of the magnetic field. This is shown in Figure 2.

In Chapter II, a theoretical approach is taken to the problem to show what information is available, and what techniques can be used to reduce the data of the experiment.

In Chapter III, the theoretical approach is examined by application of the theory to several model electron density distributions. The theory is not here substantiated by experiment since this must be done on the actual confinement device.

Chapter IV describes the construction and testing of a circular, tunable microwave vacuum window for use at 18 GHZ and above.

Chapter V discusses both the experimental determination of a suitable means to couple to the resonator for reflection and Q measurements of the resonator.

Finally, in Chapter VI, recommendations are made on ways to set up the experiment, gather data, and reduce the data.

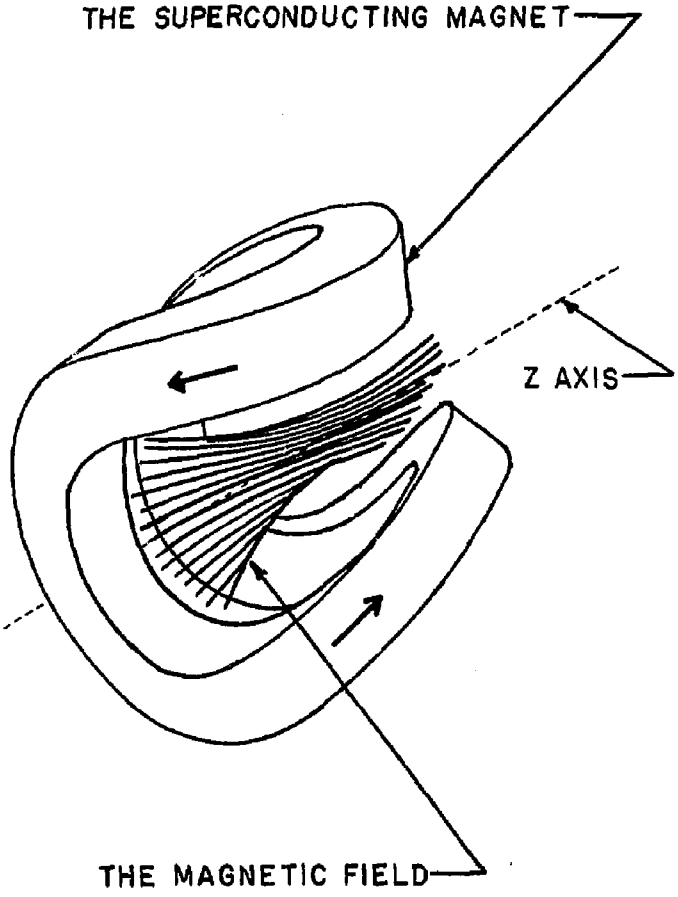

Fig. 1 The "Baseball II" Superconducting Magnet and Magnetic Field

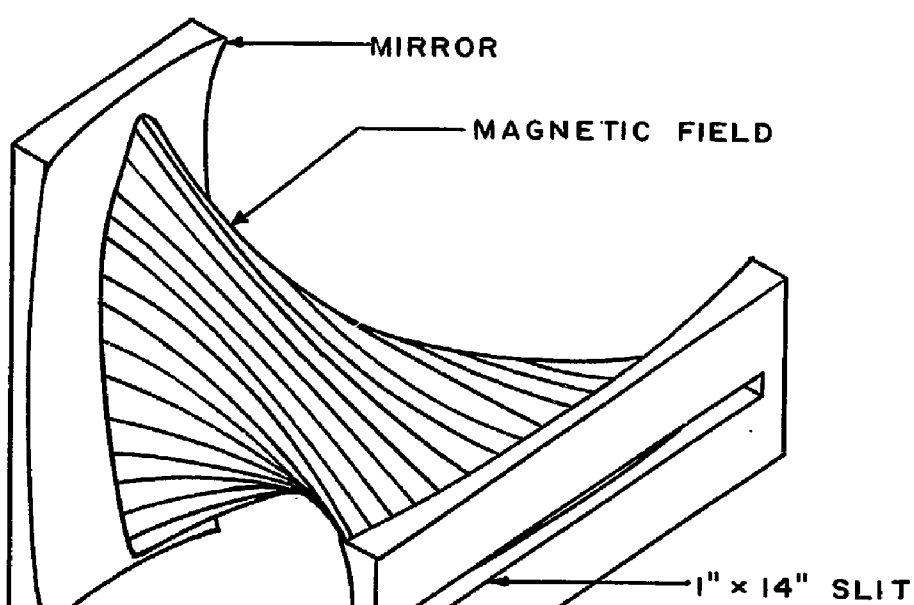

Fig. 2 Alignment of Fabry-Perot Mirrors with Respect to the Magnetic Field of the "Baseball II"

II. THEORETICAL DISCUSSION

This chapter is concerned with the information obtainable from the expected frequency shifts. A method is presented to obtain an electron density distribution by observing and analyzing several of these frequency shifts simultaneously.

ASSUMPTIONS

As with the approach of Chaffin and Beyer[9,10] to plasma diagnostics with the Fabry-Perot resonator which considers the plasma a uniform slab of thickness Δz, we must also make several assumptions about the plasma density and field configurations. These are:

1. The plasma density varies only along the axis of the interferometer, i.e.,

$$n = n(z) \tag{2}$$

2. The density distribution varies slowly as a function of z. Slowly means the density does not vary sharply within the wavelength of the probing wave.

3. The density is symmetric about the center and is a monotonically decreasing function of z, z being measured from the center of the interferometer. This provides for unique density distribution solutions.

4. The plasma does not extend to the mirrors, but exists mainly in the central portion of the reflector.

5. The confining magnetic field is parallel to the axis in the plasma volume intersected by the interferometer fields and varies only as a function of the distance along the axis.

$$B = B(z) \tag{3}$$

6. No longitudinal components of the microwave electric field exist in the resonator.

7. The electron collision frequency is much less than the difference between operating frequency and the electron cyclotron frequency.

The first assumption is an extension of the uniform distribution approximation of Chaffin and Beyer in that it allows for considering the plasma as a set of slabs, each with its own uniform density. This approach neglects the variations in the density at right angles to the axis. A refinement to this approach might be to assume that the density has a Gaussian distribution in the x and y directions.

The next three assumptions, that of a slowly varying density distribution, of a monotonically decreasing density distribution, and that of a plasma existing only near the center; all agree well with previous calculations[20] of the ion distribution assuming no spreading following trapping. These have indicated that the plasma width along the z axis at one-half its maximum density is only about 14 cm. This is shown in Figure 3. Some spreading is expected however.

The assumptions that the static magnetic field is in the z direction only, and that the microwave electric field has no longitudinal components, are required to insure that the dielectric con-

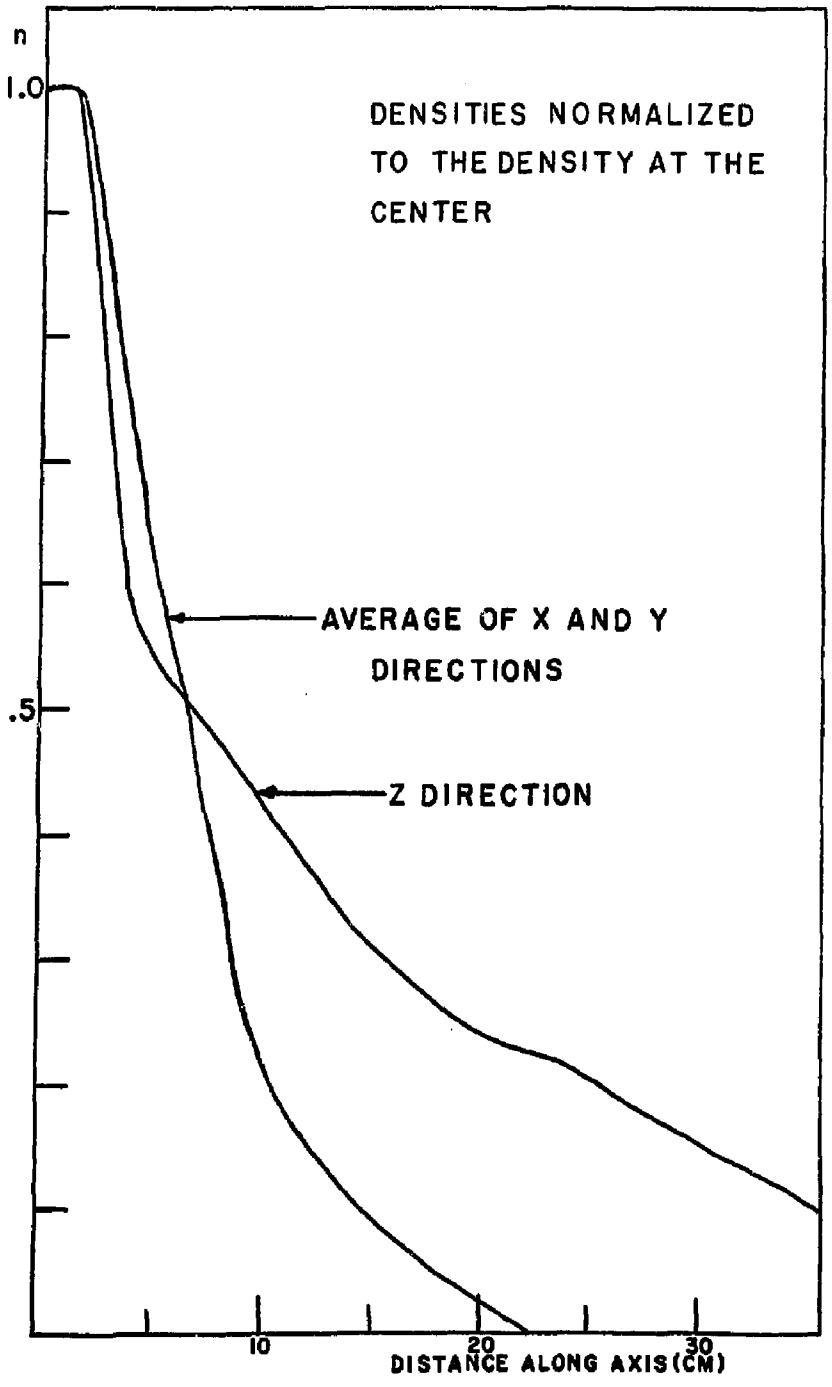

Fig. 3 Calculated Ion Density Distributions of the "Baseball II" Assuming No Spreading Following Lorentz Trapping.

stant of the plasma has the same functional form at every point on the z axis, as expressed by the Appleton-Hartree equation. By using two rectangular mirrors turned 90° from each other and oriented between the poles of the magnet as shown in Figure 2, even near the mirrors the direction of propagation of the microwave beam and the direction of the magnetic field at off-axis points are nearly parallel, although they are not parallel to the z axis. This is equivalent to the requirements of assumptions 5 and 6.

By rough calculation it is found that the collision frequency of 30 eV electrons in a plasma of 10^{10} particles/cm^3 is in the order of 10^3 sec^{-1}. This is roughly 10^7 lower in magnitude than the operating frequency and allows the last assumption to be easily met.

DETERMINATION OF THE FREQUENCY-SHIFT

A very detailed and thorough discussion of frequency shifts by perturbation theory in a resonant cavity is given by Harrington.[21] Chaffin[22] adopted his method and extended it to include anisotropic plasmas. His results are, dropping the tensor notation:

$$\frac{\Omega_1 - \Omega_0}{\Omega_0} = \frac{\int_V \Delta\tilde{\varepsilon}\vec{E}\cdot\vec{E}_0 dV}{2\int_V \varepsilon_0 \vec{E}\cdot\vec{E}_0 dV} \qquad (4)$$

where

$\Omega_0 = \omega_0(1 + \frac{j}{2Q_0})$ is defined as the complex angular resonant frequency of the unperturbed cavity.

$\Omega_1 = \omega_1(1 + \frac{j}{2Q_1})$ is defined as the complex angular resonant frequency of the perturbed cavity.

$\Delta\tilde{\varepsilon}$ is the complex change in the dielectric constant due to the presence of the plasma.

$\vec{E}$, $\vec{E}_0$ are the perturbed, unperturbed electric field vectors.

Q_1, Q_0 are the perturbed, unperturbed cavity Q's.

ω_1, ω_0 are the perturbed, unperturbed cavity resonant frequencies.

The integrals are evaluated over the space where the electric field is non-zero.

By letting $\omega_0 \simeq \omega$ and Q_0, $Q_1 >> 1$, one can separate equation (4) into its real and imaginary parts. Further assuming only a small perturbation in the electric field, set $\vec{E} \simeq \vec{E}_0$ to obtain:

$$\frac{\Delta\omega}{\omega} = \frac{\omega_1 - \omega_0}{\omega_0} = \frac{-\int_V \mathrm{Re}(\Delta\tilde{\varepsilon})|E|^2 dV}{2\int_V \varepsilon_0 |\vec{E}|^2 dV} \qquad (5)$$

$$\frac{1}{Q_1} - \frac{1}{Q_0} = \frac{-\int_V I_m(\Delta\tilde{\varepsilon})|\vec{E}|^2 dV}{\int_V \varepsilon_0 |\vec{E}|^2 dV} \qquad (6)$$

Equations (5) and (6) relate changes in the frequency and resonator Q values to the real and imaginary parts of the dielectric constant.

Heald and Wharton[23] in discussing electromagnetic radiation along the direction of a static magnetic field give an expression for the complex dielectric constant:

$$\tilde{\varepsilon}_{\ell,r} = \varepsilon_o\left[1 - \frac{\omega_p^2(\omega \pm \omega_b)}{\omega[(\omega \pm \omega_b)^2 + \nu^2]}\right] - j\varepsilon_o\left[\frac{\omega_p^2\nu}{\omega[(\omega \pm \omega_b)^2 + \nu^2]}\right] \quad (7)$$

where

ν is the electron collision frequency.

$\omega_p^2 = \frac{n(z)e^2}{\varepsilon_o m}$ is the plasma frequency.

$\omega_b = \frac{|e|B}{m}$ is the electron cyclotron frequency.

e, m is the electron charge, mass.

B_o is the static magnetic field strength.

ε_o is the dielectric permittivity constant of free space.

No generality is lost in letting B_o go to $B = B(z)$. The ℓ, r subscripts of ε designate left- and right-hand circular polarizations of the transmitted wave.[a] This result agrees with Bachynski and Gibbs[24] as well as with Allis, Buchsbaum and Bers,[25] whereas Chaffin and Beyer[9] have the denominator of the real part of the dielectric constant squared in their expression.

Circularly polarized time-harmonic fields are handled

---

[a]Some ambiguity exists as to the polarization of a wave in a resonator. If a wave traveling in the positive z direction is left circularly polarized, its reflection, which is shifted in phase by 180°, is right circularly polarized when one considers its propagation in the negative z direction. When one examines the direction of rotation of the electric field vectors with respect to the magnetic field, one observes that they are the same for both polarizations. We will therefore discuss the circular polarizations in terms of the wave traveling only in the positive z direction, and note that the right-hand wave rotates in the same sense as the gyrating electrons.

conveniently in rotating coordinates by letting

$$\vec{E}_{\ell,r} = E_x \hat{e}_1 \pm j\hat{e}_2 E_y \tag{8}$$

where $\hat{e}_1$, $\hat{e}_2$ are unit vectors in the x and y directions and the magnitude of E_x equals the magnitude of E_y. The transformation between the rectangular coordinates and the rotating coordinates can be expressed as a matrix transformation.

$$\frac{1}{\sqrt{2}} \begin{Bmatrix} 1 & -j & 0 \\ 1 & j & 0 \\ 0 & 0 & \sqrt{2} \end{Bmatrix} \begin{Bmatrix} \hat{e}_x \\ \hat{e}_y \\ \hat{e}_z \end{Bmatrix} = \begin{Bmatrix} \hat{e}_\ell \\ \hat{e}_r \\ \hat{e}_z \end{Bmatrix} \tag{9}$$

To complete equation (5), one takes the real part of the dielectric constant to obtain:

$$\frac{\Delta\omega}{\omega} = \frac{\int_V \frac{\omega_p^2(\omega \pm \omega_b)}{\omega[(\omega \pm \omega_b)^2 \pm \nu^2]} E_{\ell,r}^2 dV}{2\int_V E_{\ell,r}^2 dV} \tag{10}$$

Note that we need to consider the circularly polarized electric fields. These are expressed in terms of the x and y components of the field by equation (9). A similar approach with equation (6) relates the shift in the Q of the resonator to information about the collision frequency.

For most low density plasmas, the electron collision frequency is very much less than the microwave operating frequency, and also much less than $|\omega_b - \omega|$ unless the operating frequency is very near electron cyclotron frequency. One can neglect this term and

equation (9) is simplified to:

$$\frac{\Delta\omega}{\omega} = \frac{\int_V \frac{\omega_p^2}{\omega^2} \frac{1}{(1 \pm \frac{\omega_b}{\omega})} E_{\ell,r}^2 \, dV}{2\int_V E_{\ell,r}^2 \, dV} \qquad (11)$$

METHOD OF OBTAINING SPATIAL ELECTRON DISTRIBUTION

By remembering that ω_p^2 is proportional to $n(z)$, and that ω_b is proportional to $B(z)$, one can integrate equation (11) over x and y to obtain:

$$\Delta\omega = \int_{-b/2}^{b/2} n(z) f(\omega,z) dz \qquad (12)$$

where

$$f(\omega,z) = \frac{e^2}{2P\varepsilon_0 m\omega(1 \pm \frac{\omega_b}{\omega})} \int_{-\infty}^{\infty}\int_{-\infty}^{\infty} E_{\ell,r}^2(x,y,z)dxdy \qquad (13a)$$

and

$$P = \int_V E_{\ell,r}^2(x,y,z)dv \qquad (13b)$$

and $b = 90$ cm in our geometry and is the mirror separation.

If we apply the definition of an integral to equation (12), this result goes to a sum

$$\Delta\omega = \lim_{\Delta z \to 0} \sum_{i=1}^{\infty} n_i(z_i) f(\omega,z_i) \Delta z \qquad (14)$$

By letting the subscript i be finite, one in effect divides the density function into a step function, as shown in Figure 4. By dividing n(z) into k intervals, equation (14) is reduced to one equation with k number of unknown n_i's.

$$\Delta\omega = \Delta z(n_1 f_1 + n_2 f_2 + \ldots n_i f_i \ldots n_k f_k) = \Delta z \sum_{i=1}^{k} n_i f_i \qquad (15)$$

To solve the problem uniquely for each n_i a total of k number of equations are needed. With b = 90 cm and operating in the K band, 18 to 26.5 GHz, a maximum of 51 resonance peaks are available. By measuring the frequency shifts for each one of these resonances, one can increase the number of equations up to a maximum of 51.[a] This also establishes the limit on the possible number of n_i that can be determined. Thus, the maximum value of k is the maximum number of frequency shifts obtainable.

The complete solution can then be expressed as a set of k coupled equations. In matrix notation this is:

$$W = FN \qquad (16)$$

where

$$W = \begin{Bmatrix} \Delta\omega_1 \\ \Delta\omega_2 \\ \vdots \\ \Delta\omega_j \\ \vdots \\ \Delta\omega_k \end{Bmatrix}, \qquad N = \begin{Bmatrix} n_1 \\ n_2 \\ \vdots \\ n_i \\ \vdots \\ n_k \end{Bmatrix}$$

[a] This number can be larger if the resonator is operated at a higher band or one includes new peaks shifted into the K band by the plasma.

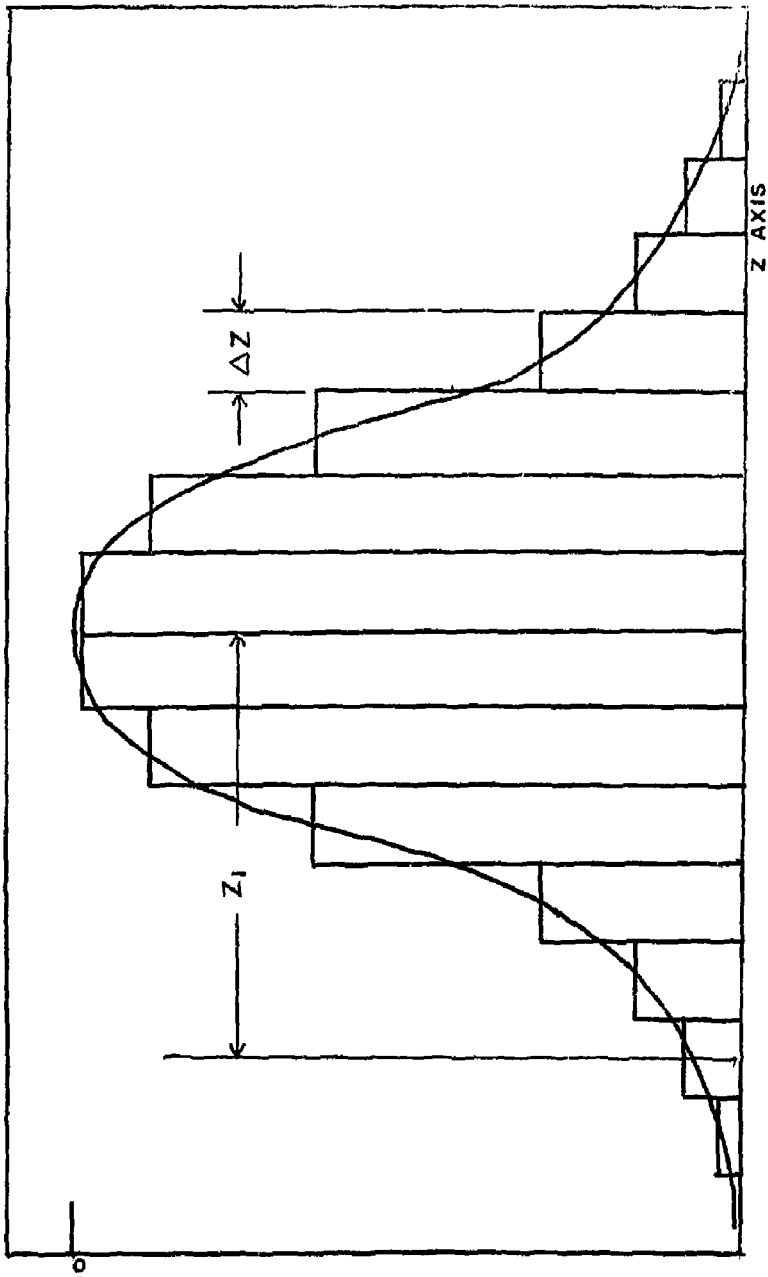

Fig. 4 Electron Density Distribution Approximated by Uniform Density Slabs

and

$$F = \Delta z \begin{Bmatrix} f_{11} & f_{12} & \cdots & f_{1i} & \cdots & f_{1k} \\ f_{21} & f_{22} & \cdots & & & \\ \vdots & & & & & \\ f_{j1} & & & & & \\ \vdots & & & & & \\ f_{k1} & \cdots & & & & f_{kk} \end{Bmatrix}$$

This is easily solved for N.

$$N = F^{-1} W \tag{17}$$

By solving for the inverse of the k by k matrix F, and by multiplying the column W by the inverse; the matrix N, and therefore each n_i, is obtained. Many cataloged computer programs exist[26] which handle this problem speedily. The only concern is in obtaining enough resolution in the frequency shift data to obtain meaningful results.

DETERMINATION OF THE ELECTRIC FIELD

The problem of determining the electric field distribution inside a Fabry-Perot interferometer is a very difficult one and a rigorous solution is yet to be found.[27] Basically one must solve the Helmholtz equation and then apply the boundary conditions. Since the resonator is mostly open and thus has unbounded surfaces, this becomes very difficult. Weinstein[15] approaches the confocal rectangular mirror resonator problem by solving the Helmholtz equation in spheroidal coordinates and by inventing quasi-rectangular coordinates to apply the boundary conditions. He discusses circular mirrors as

a good approximation to parabolic mirrors.

Boyd and Gordon,[5] Boyd and Kogelnik,[6] and Kogelnik,[16] by assuming that the dimensions of the resonator are large compared to the wavelength and that the field inside has no z component, are able to use the Fresnel-Kirchhoff formulation of Huygen's principle to find the electric field on each of the two mirrors. This is done by expressing the fields at each mirror in terms of the reflected wave from the other. For rectangular mirrors the solution for the field on one surface is:

$$E(x,y) = E_o \gamma^2 S_{om}(c,\frac{x}{a_1}) S_{on}(C,\frac{y}{A_1}) \tag{18}$$

where

$$\gamma^2 = \frac{-(-1)^{n+m}\, 4cC}{a_1 A_1 \pi^2} [R^{(1)}_{on}(C,1)]^2 [R^{(1)}_{om}(C,1)]^2 e^{-2jkb} \tag{19}$$

and

$$c = \frac{k}{b} a_1 a_2 , \qquad C = \frac{k}{b} A_1 A_2 \tag{20}$$

and $S_{oj}(s,t)$, $R^{(1)}_{oj}(s,t)$ are the angular and radial spheroidal functions. The dimensions of the mirrors are $2a_1$ by $2A_1$ and $2a_2$ by $2A_2$, as shown in Figure 5.

By approximating this solution with Hermite functions, Boyd and Kogelnik were able to derive the dimensions of the "spot" of the fundamental mode. The spot w is defined as the closed contour describing the point where the electric field intensity is reduced to $1/e$ of its maximum. This can be determined for any plane $z = z_o$ for square reflectors but is usually determined only at the mirrors and

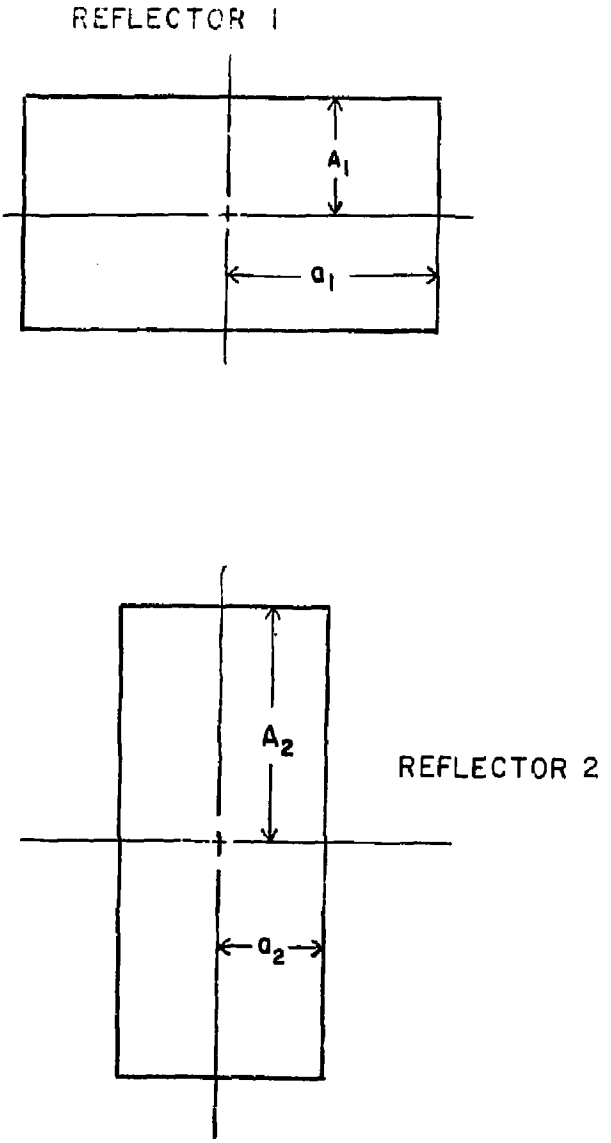

Fig. 5 Dimensions of the Rectangularly Bounded Spherical Fabry-Perot Mirrors

center of the resonator. For rectangular boundaries, the spot dimensions will be different in the x and y directions. With the subscript s meaning the spot dimensions on the surfaces of the reflectors, the spot widths are given by Boyd and Kogelnik as:

$$x_{1s} = \sqrt{\frac{a_1}{a_2}}\ \sqrt{\frac{b\lambda}{\pi}}\ , \quad y_{1s} = \sqrt{\frac{A_1}{A_2}}\ \sqrt{\frac{b\lambda}{\pi}}$$

$$x_{2s} = \sqrt{\frac{a_2}{a_1}}\ \sqrt{\frac{b\lambda}{\pi}}\ , \quad y_{2s} = \sqrt{\frac{A_2}{A_1}}\ \sqrt{\frac{b\lambda}{\pi}} \tag{21}$$

For the special case of two identical rectangular mirrors rotated 90° from each other,

$$a_1 = A_2 = g, \quad a_2 = A_1 = h \tag{22}$$

This simplifies equations (21) to:

$$x_{1s} = y_{2s} = \sqrt{\frac{g}{h}}\ \sqrt{\frac{b\lambda}{\pi}}$$

$$y_{1s} = x_{2s} = \sqrt{\frac{h}{g}}\ \sqrt{\frac{b\lambda}{\pi}} \tag{23}$$

Typical values of the spot size in centimeters on the surface of the reflector with b = 90 cm, and g = 5 in. and h = 8 in., are:

$\omega/2\pi$ =	18.0 GHz	26.5 GHz	40.0 GHz
x_s =	5.48	4.53	3.68
y_s =	8.76	7.20	5.79

The position of the minimum field width is in general different for the electric fields in the x and y directions. This position, which is at the center of the resonator for square mirrors, is shifted an amount D_x, D_y along the z axis towards the smaller reflector for crossed rectangular mirrors. This amount is:

$$|D_x| = |D_y| = \frac{b}{2} \frac{|g^2 - h^2|}{g^2 + h^2} \tag{24}$$

For the same dimensions cited above, the displacement of the maximum energy density position from the center along the z axis is 24.8 cm.

The spot dimensions in the x and y directions at the position of maximum energy density of the microwave field are found by:

$$x_0 = y_0 = \sqrt{\frac{x_s y_s}{2}} = \sqrt{\frac{b\lambda}{2\pi}} \tag{25}$$

It should be noted that the minimum spot widths for the x and y directions do not occur at the same place but are opposite of the center of the resonator from each other. For the same dimensions previously used, values of the spot width minima in centimeters are:

$\omega/2\pi$ =	18.0 GHz	26.5 GHz	40.0 GHz
$x_0 = y_0$ =	4.87	3.98	3.12

These correspond to the spot widths produced at the center by a square boundary reflector with dimensions of $2a_0$ by $2a_0$, where $a_0 = \sqrt{gh}$. Figure 6 shows the spot width configuration for this example.

Two more things can be deduced from the solution of the electric field.

1. The resonance condition is

$$\frac{4b}{\lambda} = q + 1 \tag{26}$$

for the TEM_{ooq} modes. It can be shown from equation (19) that the diffraction losses from the higher order modes are much greater. For this reason only the ooq modes are considered in the electric field solutions.

2. The diffraction losses of a confocal system with unequal reflector sizes of dimensions a_1, A_1, a_2, and A_2 are equal to the diffraction losses of a confocal system with equal reflector dimensions of a_0, A_0 if $a_0^2 = a_1 a_2$ and $A_0^2 = A_1 A_2$. Kogelnik[27] calls these "equivalent systems." For our geometry the equivalent system would be a square reflector with dimensions $a_0^2 = A_0^2 = gh$ or $a_0 = 6.34$ in. = 16.1 cm.

The spot sizes for the square boundary spherical mirrors are found in the same way as with the rectangular mirrors.

$$w_s = \sqrt{x_s y_s} = \sqrt{\frac{b\lambda}{\pi}} \tag{27}$$

and

$$w_0 = w_s/\sqrt{2} \tag{28}$$

Notice that this is independent of the size of the mirrors. Also, the minimum spot size occurs in the center, as one would expect. Values for the spot size in centimeters with b = 90 cm are:

$\omega/2\pi$ =	18.0 GHz	26.5 GHz	40.0 GHz
w_s =	6.95	5.66	4.62
w_o =	4.87	3.98	3.25

Figure 7 depicts this graphically.

To find the electric field at any point between the mirrors Huygen's principle is again used. The resulting integral can only be integrated by approximating the spheroidal functions with Gaussian-Hermite functions in the limit as $c \to \infty$, where c was defined in equation (20). This condition requires that the dimensions of the reflector be large with respect to the wavelength. For a square reflector of dimensions a_o given above, the values of c at several frequencies are:

$\omega/2\pi$ =	18.0 GHz	26.5 GHz	40.0 GHz
c =	10.9	16.1	24.3

Clearly some error is produced with this approximation.

Boyd and Gordon[28] show the value of $E_x(x,y,z)$ to be:

$$E_x(x,y,z) = E_o\sqrt{\frac{2}{1+\xi^2}}\ \frac{\Gamma(\frac{m}{2}+1)\Gamma(\frac{n}{2}+1)}{\Gamma(m+1)\Gamma(n+1)}\ H_m(X\sqrt{\frac{2}{1+\xi^2}})$$

$$\cdot\ H_n(Y\sqrt{\frac{2}{1+\xi^2}})\ \exp[-\frac{kw^2}{b(1+\xi^2)}] \qquad (29)$$

$$\cdot\ \exp(-j\{k[\frac{b}{2}(1+\xi)+\frac{\xi}{1+\xi^2}\ \frac{w^2}{b}] - (1+m+n)(\frac{\pi}{2}-\phi)\})$$

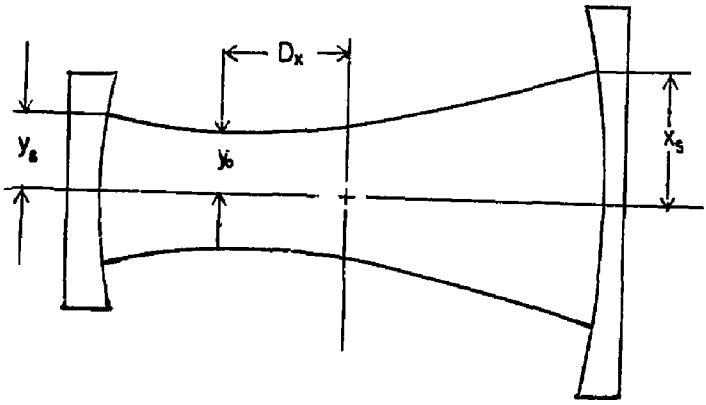

Fig. 6 The Spot Size for Crossed Rectangular Reflectors

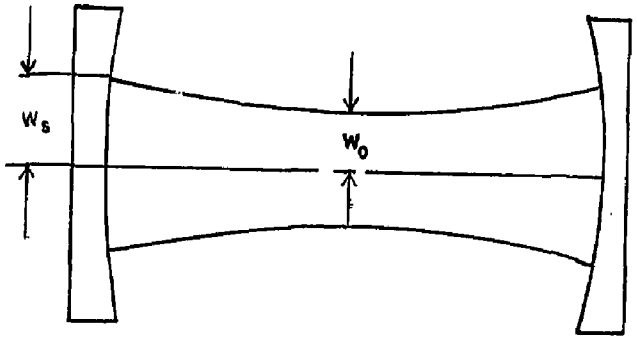

Fig. 7 The Spot Size for Square Reflectors

where

$$x = \frac{x\sqrt{c}}{a_o}, \quad y = \frac{y\sqrt{c}}{a}$$

$$c = \frac{k}{b} a_o^2 = \frac{k}{b} gh$$

$$w^2 = x^2 + y^2 \tag{30}$$

$$\xi = \frac{2z}{b}$$

$$\phi = \tan^{-1} \frac{1 - \xi}{1 + \xi}$$

$$E_o = E_x(0, 0, 0)$$

and H_n and H_m are the Hermite polynomials. If n,m = 0, as is the case for the TEM_{ooq} modes, the Hermite polynomial $H_o(x) = 1$, and equation (29) can be simplified to:

$$E_x(x,y,z) = E_o \exp\left[\frac{-kw^2}{b(1 + \xi^2)}\right] \exp\left(-j\left\{k\left[\frac{b}{2}(1 + \xi) + \frac{\xi}{1 + \xi^2} \frac{w^2}{b}\right]\right.\right. \tag{31}$$

$$\left.\left. - \left(\frac{\pi}{2} - \phi\right)\right\}\right)$$

To obtain the right- and left-hand circularly polarized fields needed for equation (13a), one needs to use equation (8) and note that by symmetry $E_x = E_y$. $E^2_{\ell,r}(x,y,z)$ is found to be:

$$E^2_{\ell,r} = E^2_x \tag{32}$$

This fully determines the sensitivity function $f(\omega, z)$ in equation (13a). By measuring the frequency shifts one should be able to deduce the density distribution. It remains to show what the magnitudes of the resonant frequency shifts will be.

III. FREQUENCY SHIFT MAGNITUDES AND SPATIAL SENSITIVITIES

In this chapter numerical plots are given of the frequency shifts due to assumed density distributions, and the spatial variation in the sensitivity of the Fabry-Perot resonator to electron densities. This is done for the 18 to 26.5 GHz frequency range and a magnetic field strength which produces an electron cyclotron frequency slightly higher at the center of Baseball II.

APPROXIMATIONS

To obtain "ballpark" estimates of the expected frequency shifts and sensitivities, it is advisable to make the following assumptions:

1. The microwave field region intersects a cylindrical region of the plasma volume which has only axial variation of electron density.

2. The microwave electric field intensity does not vary with z between the mirrors. This is equivalent to assuming that the axial variation of the electron density is small over a half wavelength.

3. The static magnetic field varies about the center of the interferometer axis in the z direction as:

$$B(z) = B_c[1 + (z/\beta)^2]\text{Tesla} \qquad (33)$$

where B_c is the magnetic field strength at the center and β is empirically found to be 36.2 cm. This is determined from the magnet design curves and is very close to the design curve for $|z| \leq 35$ cm. This is shown in Figure 8 as the dotted line.

With these approximations equation (11) assumes the following form:

$$\Delta\omega = \frac{1}{2b} \int_{-b/2}^{b/2} \frac{\omega_p^2 dz}{\omega(1 \pm \frac{\omega_b}{\omega})} \qquad (34)$$

Since the right-hand circular polarization that gyrates in the same sense as the gyrating electrons introduces a *minus* sign in the denominator which allows the frequency shift to become large as ω approaches ω_b, we will consider only this polarization at this time. The left hand polarization will be relatively ineffective in yielding information about the spatial distribution of n_e.

FREQUENCY SHIFT MAGNITUDES

In this section two different density distributions will be considered with each having the same line density along the axis. They are the uniform slab and a triangular distribution.

Uniform Slab Approximation

The plasma electron distribution can be roughly approximated by a slab of density n_0 and width $2\Delta z_0$ centered about $z = 0$. Equation (34) becomes:

$$\Delta f_s = A \int_0^{\Delta z_0} \frac{dz}{\gamma^2 + z^2} \qquad (35)$$

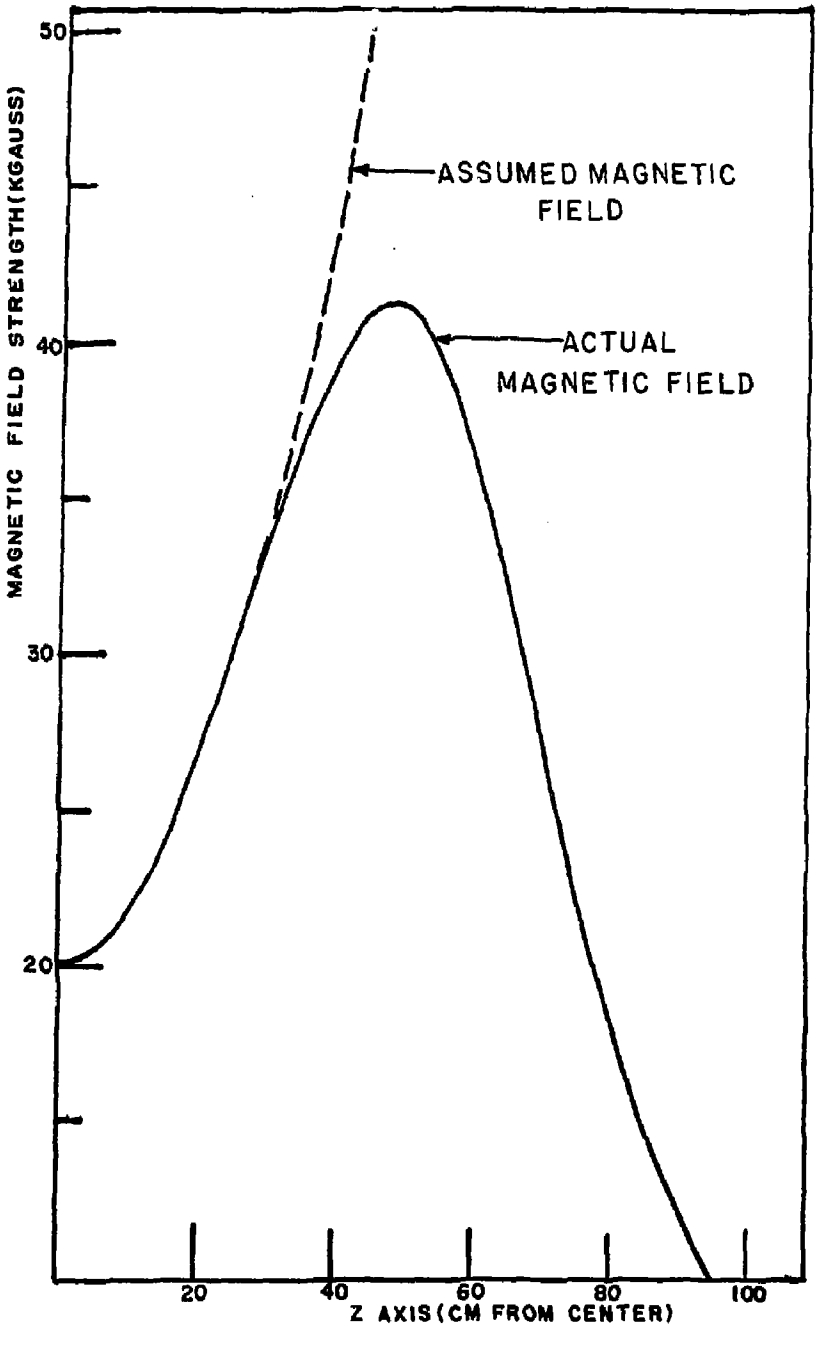

Fig. 8 Magnetic Field Strength along the Z Axis of the "Baseball II"

where

$$A = \frac{-n_o e\beta^2}{2\pi b \varepsilon_o B_c} ,$$

$$\gamma^2 = \frac{(eB_c - m\omega)\beta^2}{eB_c} ,$$

and for this model the slab half-width will be taken as:

$$\Delta z_o = 7.24 \text{ cm.}$$

For γ^2 to be a real, positive constant, the operating frequency ω must be less than the electron cyclotron frequency ω_b. It is possible to handle the case of $\omega > \omega_b$ but then the propagation constant of the wave through the plasma is complex and the wave is attenuated.

The integral is easily evaluated to give the following expression for the frequency shift:

$$\Delta f_s = \frac{A}{\gamma} \tan^{-1}\left(\frac{\Delta z_o}{\gamma}\right) \qquad (36)$$

for $\omega < \omega_b$

Triangle Approximations

The density might also be approximated by:

$$n = n_o\left[1 - \left(\frac{z}{2\Delta z_o}\right)\right], \quad 0 \leq z \leq 2\Delta z_o \qquad (37)$$

where Δz_o is the same as in the previous example. The frequency shift takes a slightly different form but with the same constants:

$$\Delta f = A \int_0^{2\Delta z_o} \frac{\left[1 - \left(\frac{z}{2\Delta z_o}\right)\right] dz}{\gamma^2 + z^2} \qquad (38)$$

Upon integrating, the following is obtained:

$$\Delta f = A\{\frac{1}{\gamma}\tan^{-1}(\frac{2\Delta z_o}{\gamma}) - \frac{1}{4\Delta z_o}\ln[\frac{\gamma^2 + 4(\Delta z_o)^2}{\gamma^2}]\} \qquad (39)$$

$$\omega < \omega_b$$

In Figure 9 the frequency shifts of the triangular and slab distributions are plotted and compared as a function of ω_b/ω. By adjusting the peak density, it is possible to also consider a somewhat wider triangular distributions having the same line density. This was done and plotted in Figure 10 for $\Delta z_2 = 2\Delta z_o$, $\Delta z_4 = 4\Delta z_o$, and $\Delta z_6 = 6\Delta z_o$, where $\Delta z_2, \Delta z_4, \Delta z_6$ are the widths of the distributions from the center. The electron cyclotron resonance frequency at the center is 26.5 GHz for this example.

SPATIAL SENSITIVITY

One can determine the spatial sensitivity of the Fabry-Perot interferometer by considering a thin slab of electrons of thickness Δa and density N_o placed at an arbitrary plane $z \quad z_o'$. One can then examine the frequency shift as a function of z_o' for several different frequencies. The frequency shift caused by the slab is expressed by the following integral:

$$\Delta f = \frac{A'}{2} \int_{z_o' - \Delta a/2}^{z_o' + \Delta a/2} \frac{dz}{\gamma^2 + z^2} \qquad (40)$$

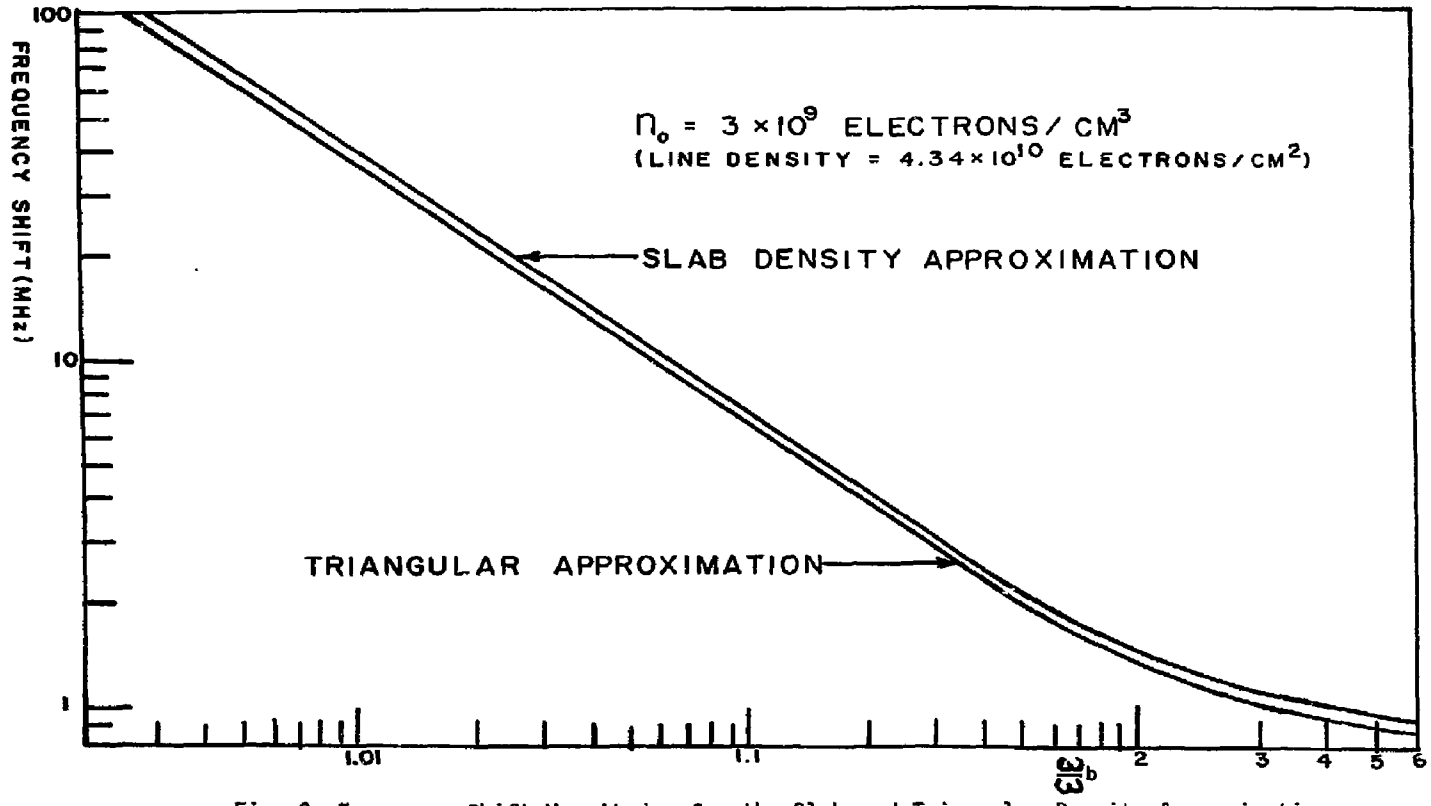

Fig. 9 Frequency Shift Magnitudes for the Slab and Triangular Density Approximations

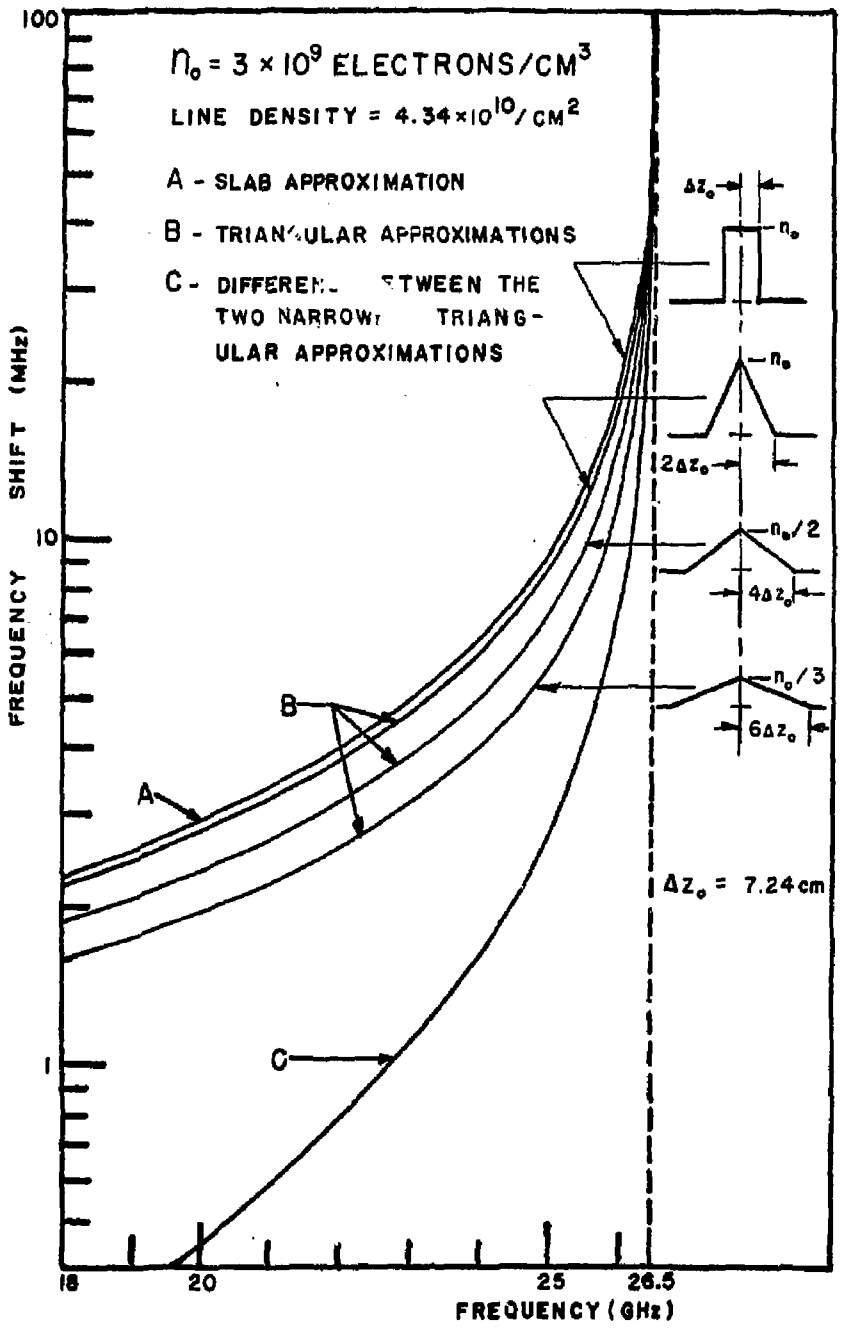

Fig. 10 Frequency Shift Magnitudes for Four-Density Distributions having the Same Line Density

where

$$A' = \frac{N_o}{n_o} A,$$

and A and γ are the same as in the previous examples. By integrating, the expression for the frequency shift becomes:

$$\Delta f = \frac{A'}{2\gamma} \left[\tan^{-1}\left(\frac{z_o' + \Delta a/2}{\gamma}\right) - \tan^{-1}\left(\frac{z_o' - \Delta a/2}{\gamma}\right)\right] \qquad (41)$$

Furthermore, to obtain the same magnitude of numbers, as in the previous result, we can require that the line density along the axis is the same. This forces N_o to assume the value:

$$N_o = 2n_o \frac{\Delta z_o}{\Delta a} \qquad (42)$$

The frequency shift as a function of $z = z_o'$ is plotted for several different frequencies in Figure 11. These plots show the fundamental feature on which the proposed measurements are based, i.e., that the spatial sensitivity of the microwaves to the plasma density is frequency dependent.

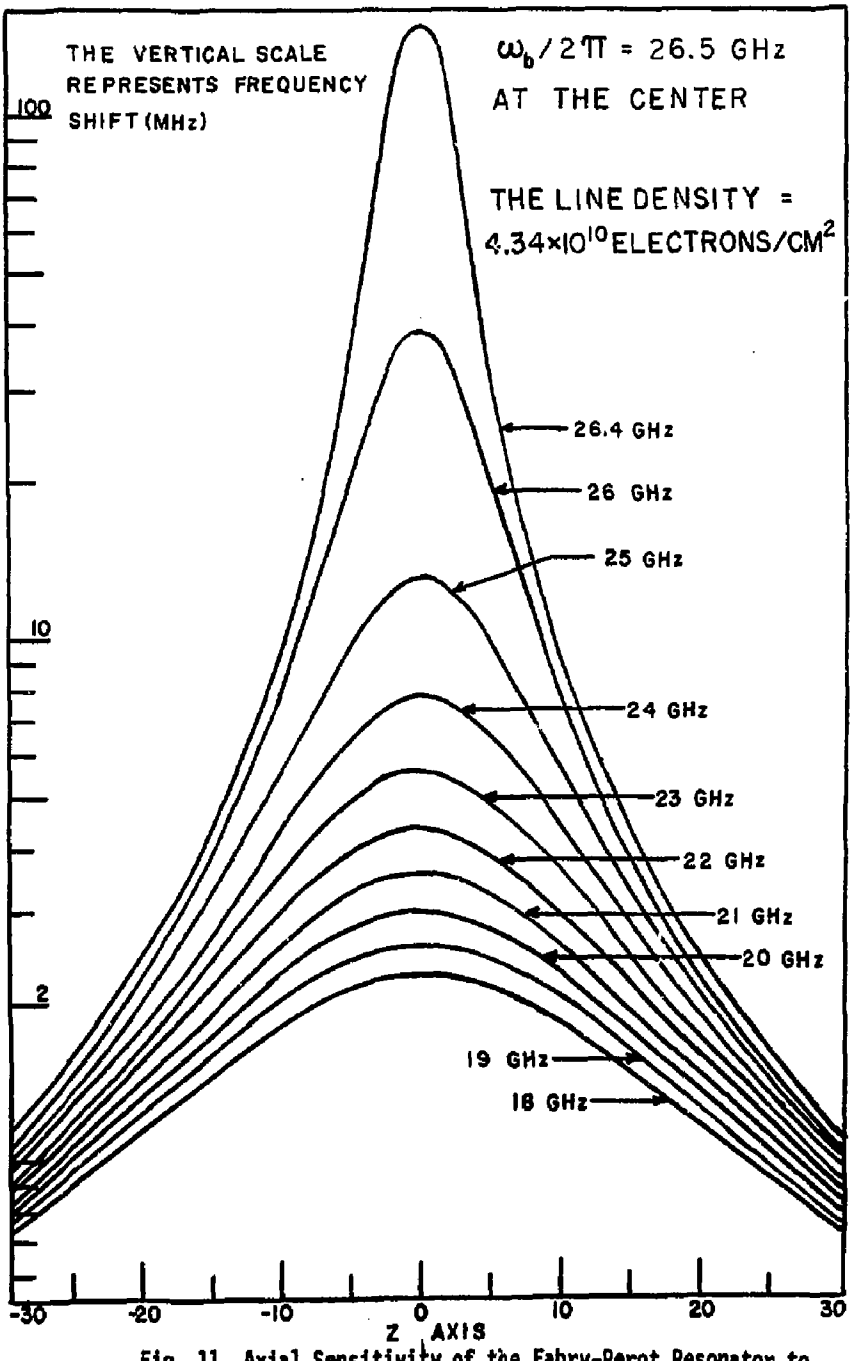

Fig. 11 Axial Sensitivity of the Fabry-Perot Resonator to a Uniform Density Plasma Slab at Various Frequencies

IV. CONSTRUCTION AND TESTING OF THE MICROWAVE VACUUM WINDOW

The diagnosis of the circularly polarized waves outside the vessel containing the plasma and the superconducting magnet is simplified if one can use a circular microwave vacuum window mounted in a cylindrical waveguide. This type of device is not commercially available. The following discusses the method of operation and the characteristics of tunable, fairly broad-band double window.

METHOD OF OPERATION

The window simply consists of two circular waveguides with dielectric disks sealed in each end and separated from their centers by a distance equal to one quarter of the guide wavelength of the transmitted wave. The window can then be tuned by varying the waveguide separation between the ends. The waveguides are connected by a toroidally-shaped spring whose minor diameter is much greater than the waveguide separation. The spring drops partially into the gap between the waveguide ends and becomes in effect a waveguide between the two ends. This is shown in Figure 12.

Since there are two disk seals in the waveguide it is possible to provide a guard vacuum for protection in the event one of them ruptures. This, along with the tunability of the window, resulted in the present design. Figure 13 shows an assembly drawing of the window and Figure 14 shows the completed model which was tested. Detailed drawings of each part are given in Appendix A. The vacuum

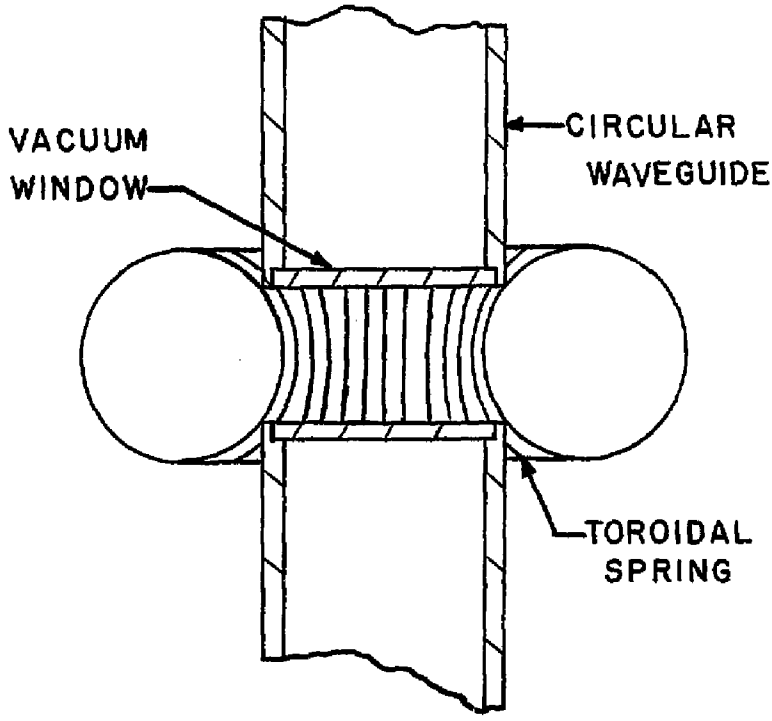

Fig. 12 Toroidal Spring Providing Electrical Contact between the Circular Waveguide of the Vacuum Window

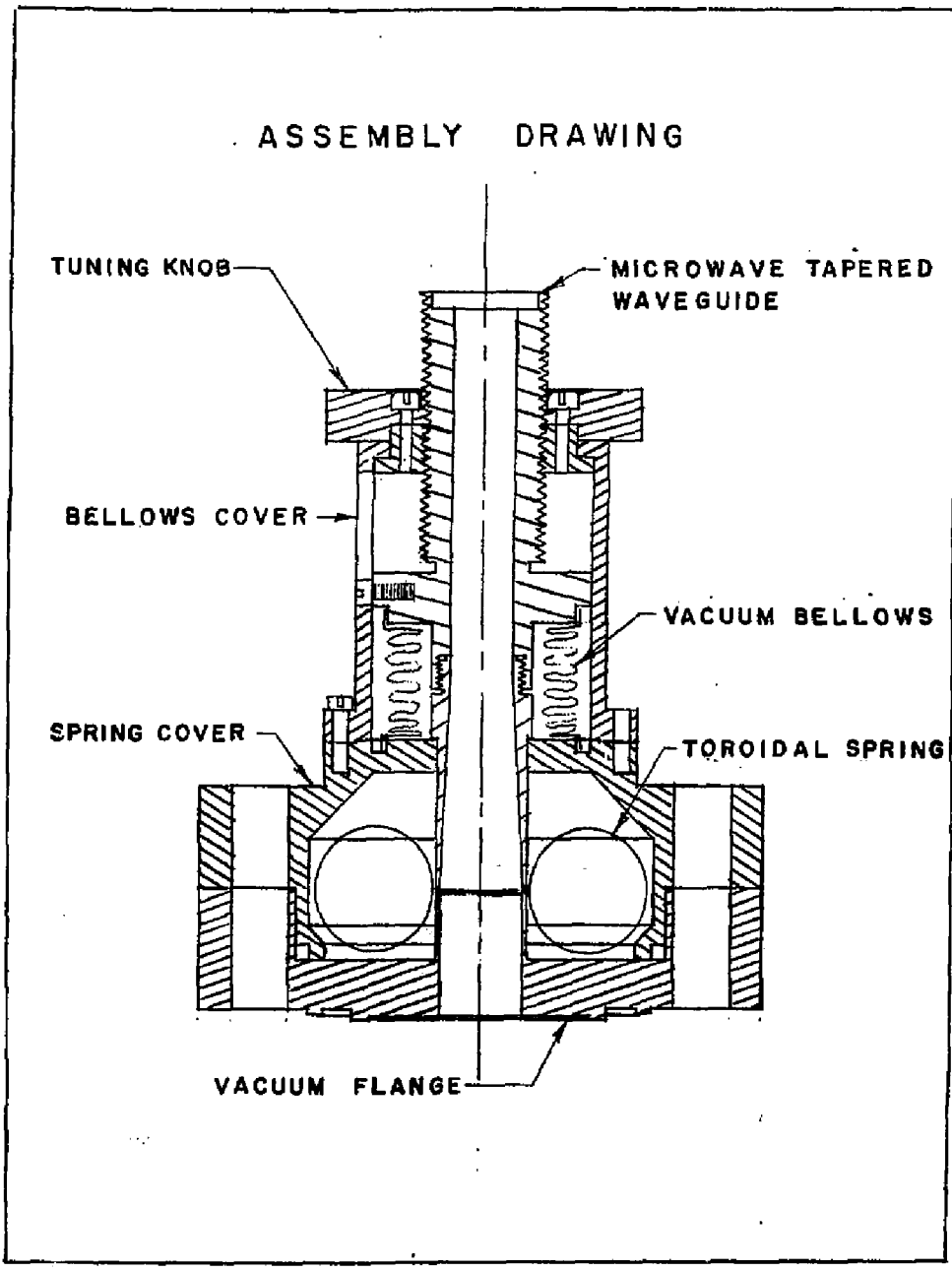

Fig. 13 Cross-sectional View of the Assembled Vacuum Window

flange was designed to be compatable with the flanges at Livermore, and the waveguide input is compatable with the DeMornay-Bonardi DBE-030 rectangular to circular waveguide K-band transmission.

Both quartz and ceramic disks were tested as vacuum windows. They both had the same thickness but different diameters. For this reason two separate versions of the window were built. The ceramic has high power dissipation capabilities and a high dielectric constant, and the quartz, on the other hand, has a lower dielectric constant, resulting in reduced reflection.

TEST TECHNIQUES

The main method of testing was to observe the reflection characteristics and hence infer the transmission by swept-frequency measurements of the voltage standing wave ratio (VSWR). Such a measurement is a standard technique in microwave engineering where the VSWR is defined as:

$$VSWR = \frac{V_{max}}{V_{min}} = \frac{V_i + V_r}{V_i - V_r} \tag{42}$$

where V_i, V_r are the incident and reflected wave voltage amplitudes. The voltage ratio is measured with a movable crystal detector probe in a waveguide slotted line. This is related to the voltage reflection coefficient ρ by:

$$\rho = \frac{V_r}{V_i} = \frac{VSWR - 1}{VSWR + 1} \tag{43}$$

The power transmission coefficient T is related to ρ, assuming no appreciable losses, by the following:

$$T = 1 - \rho^2 = \frac{4\ VSWR}{(VSWR + 1)^2} \qquad (44)$$

Clearly, the optimum transmission and least reflection is obtained when the standing wave ratio is nearest unity.

To plot the VSWR of a device over a range of frequencies by determining the VSWR at each separate frequency would be very laborious. By sweeping the frequency across the range rapidly, while viewing the detector output as the detector is slowly moved along the slotted line, one sees the detector output trace a smear envelope as seen in Figure 15. A memory device such as a memory oscilloscope, an x-y recorder, or a photographic time exposure, is needed to record this information.

For low power application, the voltage output of a crystal detector is proportional to the square of the microwave voltage. Thus, the VSWR is the square-root of the ratio of the maximum to minimum voltages of the smear envelope, as seen from the detector output.

$$VSWR = \sqrt{\frac{x_{max}}{x_{min}}} \qquad (45)$$

Using this result one can easily obtain the reflection and transmission characteristics of any microwave device over the range at which the sweep oscillator is operating.

DEVELOPMENT

This section discusses the reasons for choosing quartz as a vacuum window, and the method found to make the springs to provide electrical contact between the waveguide ends.

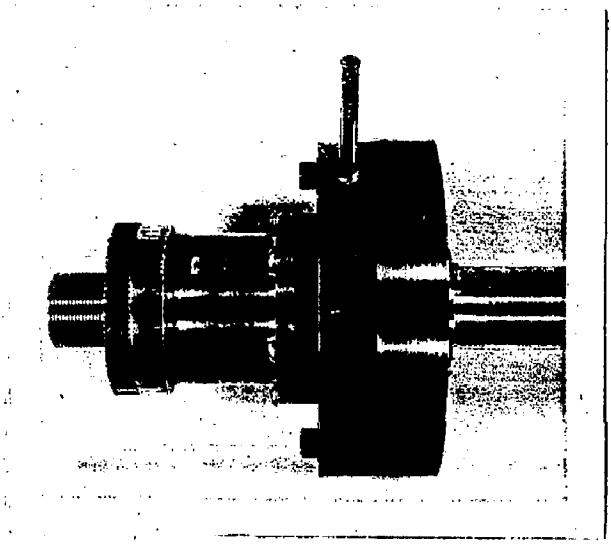

Fig. 14 The Completed Vacuum Window

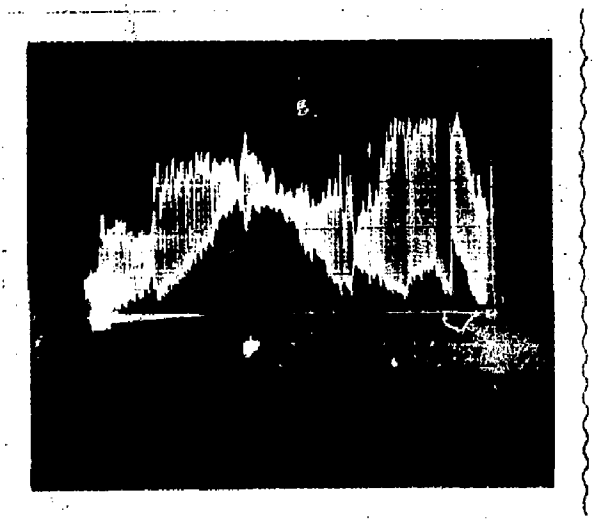

Fig. 15 A typical Swept Frequency Standing Wave Envelope

The Vacuum Windows

Both quartz and ceramic disks were considered for use as the vacuum windows. The ceramic disk was first considered because of its ruggedness and ability to withstand higher temperatures, as would be needed for brazing. As the vacuum restrictions of the "Baseball II" were eased, it was thought that a quartz window might be preferable because of its lower dielectric constant and resulting wider bandwidth and higher transmission. Since this experiment is concerned with data observable over the whole band, it was decided to use the quartz windows in the final test device although two flanges with ceramic disks installed were previously constructed.

VSWR tests were also made on each disk material to determine its transmission and bandwidth characteristics, using both single and double thicknesses. In the double thickness tests, the two disks were separated by a quarter wavelength to simulate the final mode of the window. A comparison of the two disks is shown in Figure 16. Note that the bandwidth of the ceramic disk is about one-half that of the quartz disk. The quartz disk and the ceramic disks were also compared in both models of the completed window and similar results were obtained.

The disk was sealed in the waveguide by applying a small bead of TORRSEAL (a vacuum grade epoxy made by Varian) to the edges. There was some concern that the epoxy bead might affect the microwave characteristics of the window, but no difference was detectable.

The Toroidal Spring

Phosphor-Bronze wire of various gauges was tested for the toroidal spring to provide electrical contact between the two waveguide

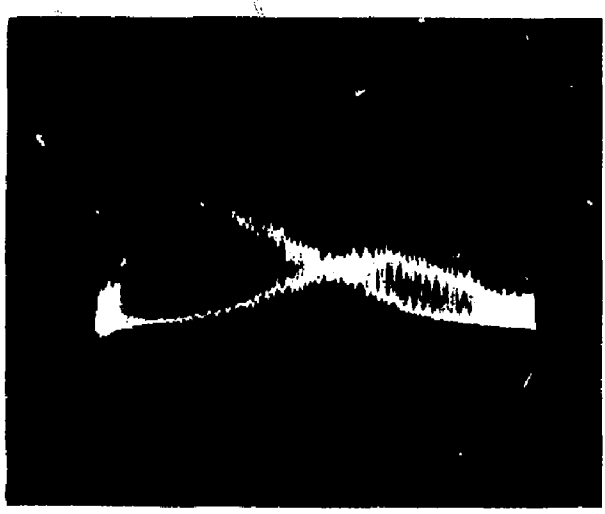

CERAMIC

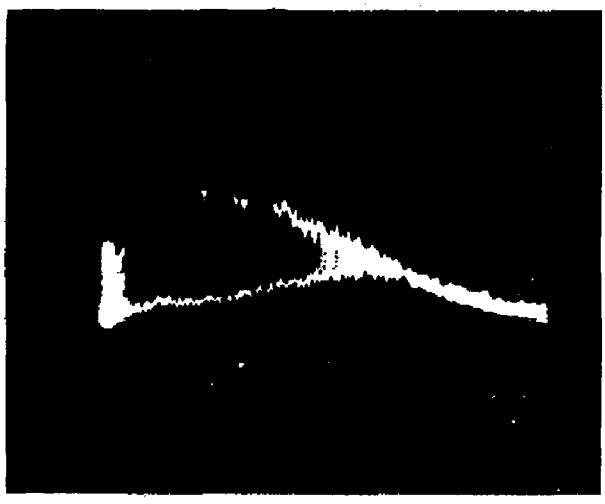

QUARTZ

Fig. 16 Swept Frequency Standing Wave Envelope for Double Quartz and Ceramic Windows

ends. The problem was to provide a firm contact, with the minimum space between windings of the spring, and to make the minor diameter of the spring large compared to the wavelength so that it would not drop too deeply into the gap between the two waveguide ends. The minor diameter is the diameter of the spring before the ends are soldered together. The major diameter is the diameter of the resulting torus.

A problem was found with large, fine-wire springs in that they easily collapse in the azimuthal direction so that the individual turns are no longer in the plane of the torus axis, and the minor cross section is no longer circular. In the collapsed condition they do not drop into the gap as the window is tuned. This problem is avoided by using a heavier gauge wire and/or smaller minor diameters of the spring. The thickness of the wire used in the final spring is 0.030 in., and the minor diameter of the torus is 0.62 in.

The spring is constructed by first winding the spring wire using a slowly turning metal lathe, and then bending the spring around so that the ends are flush with each other. One complete turn of each end is then soldered to the corresponding turn on the other end. In positioning the spring for soldering it was found most convenient to place spacers between each winding along one side until the ends are curved around enough to touch each other. Figure 17 shows this process and a completed spring.

The length of the spring before bending is determined by requiring that the toroidal spring be nearly relaxed and have its windings almost touching each other on the inner side when the window is tuned to its lowest frequency. The spring length used in the completed window is 1.73 in.

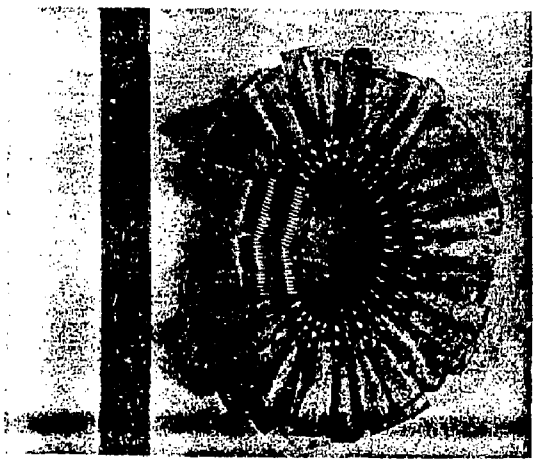

SPACERS BENDING THE SPRING ALLOW EASY SOLDERING

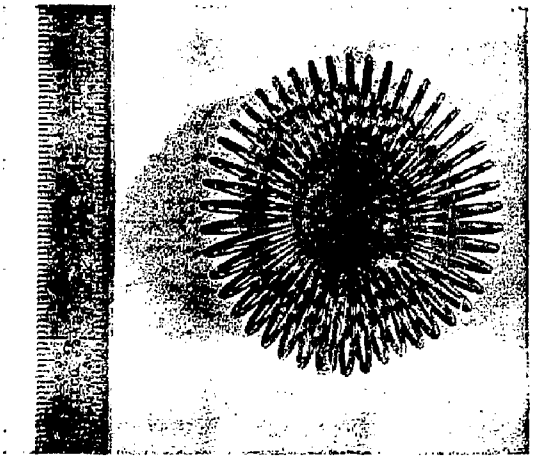

THE COMPLETED SPRING

Fig. 17 The Toroidal Spring

Spring Cavity Resonances

When the microwave window is operated without a spring, several sharp reflection peaks are observed in the frequency spectrum. These peaks are also apparent to a lesser extent with the spring in place (see Figure 18). These peaks are hence attributed to those resonances of the cavity in which the spring is enclosed to which waves may couple through the spring. By placing a microwave absorber along the cavity walls, these peaks are greatly reduced. Figure 19a shows the resulting VSWR plot without the spring, and Figure 19b is with the spring in place. The absorber is "Eccosorb" AN-73 with one of three layers removed. Because of the thickness of the absorber and the limited space in the spring cavity, it is suggested that a thinner absorber such as "Eccosorb" AN-72, be used.

VACUUM WINDOW TESTS

The microwave characteristics of the vacuum window were tested extensively from 18.0 GHz to 26.5 GHz, since this was the frequency range of available equipment. By considering the quartz disks in the waveguide ends to be nearly touching, one is able to estimate the frequency whose dielectric half-wavelength in the guide equals the thickness of the two disks. This establishes an upper limit for transmission of about 31.5 GHz. Above this the window could be tuned for the separation of the centers equal to 3/4 of a guide wavelength, although the bandwidth would be smaller. The cut-off frequency for the waveguide used is 14.7 GHz for the TE_{01} mode. This is the lowest possible frequency which one might use. The following will discuss the microwave and vacuum characteristics of the window.

WITHOUT SPRING OR ABSORBER

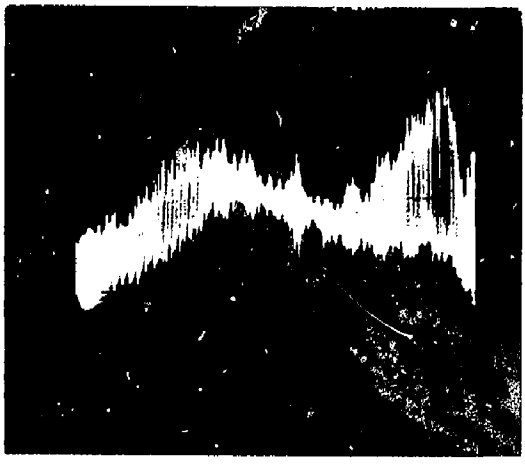

WITH SPRING ONLY

Fig. 18 Spring Cavity Resonances of the Vacuum Window

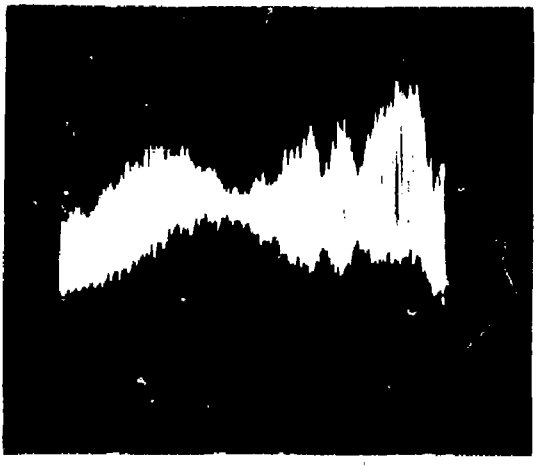

A. ABSORBER ONLY

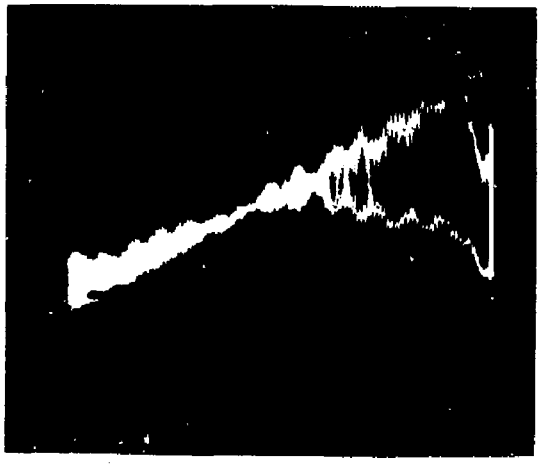

B. WITH ABSORBER AND SPRING

Fig. 19 Effect of Microwave Absorber on Spring Cavity Resonances

Microwave Tests

The swept-frequency VSWR measurement technique was used to measure the transmission and tunability of the vacuum window. The window was connected to a microwave slotted-line through a rectangular to circular transition, and a circular horn was placed on the far side of the window to launch the transmitted power. This was absorbed by a microwave absorber so that essentially no signal was reflected. This is shown schematically in Figure 20. The time exposure photo of the oscilloscope display of the resulting smear analysis is shown for several settings of the window tuning in Appendix B for both quartz and ceramic disks. A scale is attached to the tuning knob of the window tuning mechanism to read the nearest hundredth of a turn. Each completed turn of the knob represents 1/20th of an inch movement in the waveguide. For the window tuned to the center of the band, the VSWR was found to be slightly less than 1.1 at the center and about 2.2 at the two extremes. This was also determined independently using a Hewlet-Packard SWR meter, HP 415E. This represents a power transmission of 99.8 percent in the center and about 86 percent at the extremes. By plotting the smear envelope with an x-y recorder, and by calculating and plotting the VSWR at each point by equation (45), one obtains a chart showing the VSWR as a function of frequency. This is plotted on a logarithmic scale in Figure 21 for the window at the setting of 1.10 turns. Plots of the VSWR at other settings are given in Appendix C.

Vacuum Tests

The window is designed to be differentially pumped to guard against small leaks. It was leak tested down to 10^{-7} torr as the

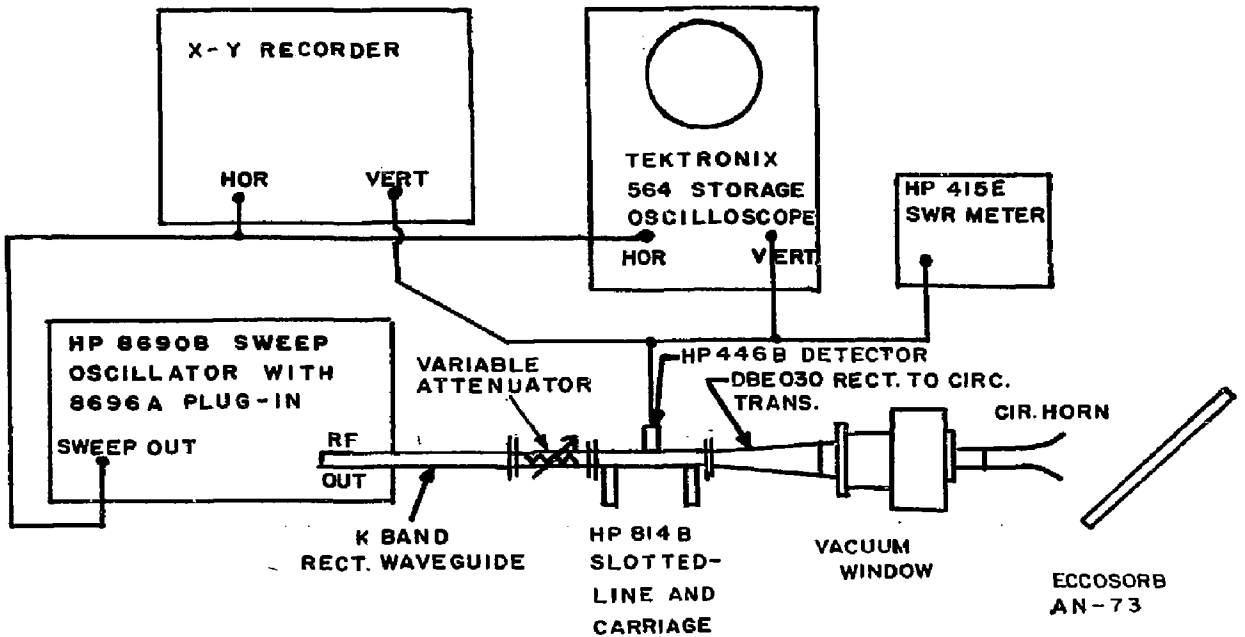

Fig. 20 Vacuum Window Testing Technique

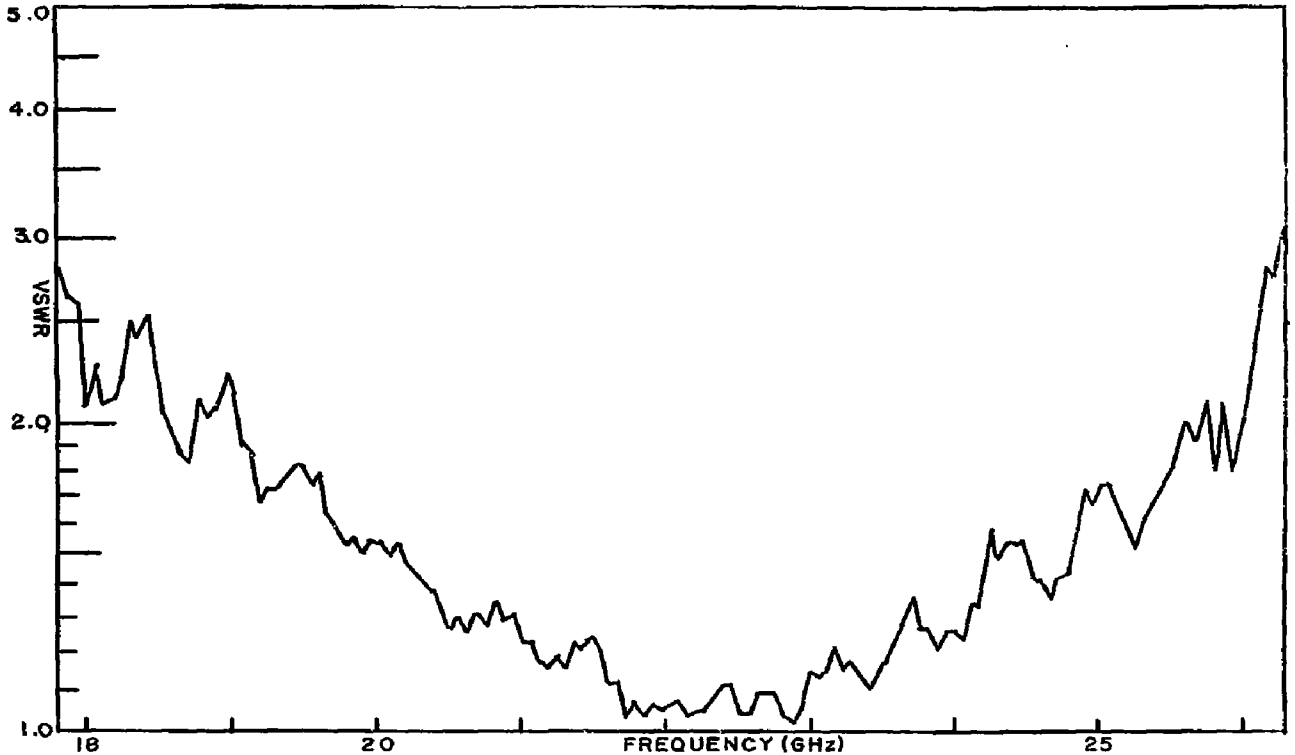

Fig. 21 Frequency Dependence of the VSWR for the Vacuum Window Tuned to 1.10 Turns

individual parts were sealed, and again after it was completely sealed. No leaks were detected.

To determine the strength of the quartz disk and seal, a single disk was sealed in a seat with the same dimensions as the waveguide seat in the window and put under pressure. The window was tested up to 67 lbs/in.^{2} without breaking.

V. COUPLING OF THE RESONATOR

As an introduction to the discussion of the coupling of the microwave signal in and out of the resonator, a brief discussion of the alignment of the interferometer is given.

ALIGNMENT OF THE RESONATOR

Two spherical mirrors of equal radii are said to be confocal if the center of curvature of each lies on the surface of the opposing mirror. This is the same as saying that the focus of each mirror is at the same point.

To obtain the proper alignment of reflectors, the reflectors are set up at approximately one radius apart. If one looks at the frequency spectrum of the resonant peaks, one notices that each peak is usually split into many smaller ones. By moving one mirror back and forth along the axis of the resonator, one sees that at one point all of the smaller peaks degenerate into one large peak. At this point the mirrors are separated by their radius. By tilting each of the mirrors at this separation one can observe an extra set of resonances half-way between the larger resonances. The mirrors remain confocal during tilting, but the coupling iris moves off the axis. Thus a wave undergoes three reflections which doubles the path length before being refocused on the iris. By adjusting the tilt of both mirrors one can make these resonances disappear completely. When this is done, the resonator is aligned with the coupling iris located at the

center of curvature of the opposite mirror.

WAVEGUIDE COUPLING

Although it would be easier to detect the resonances by observing the transmission output of the resonator, this would require a second vacuum window and would interfere with other measurements on the "Baseball II". Furthermore, other considerations require a lengthwise slit, one inch wide, centered in one of the reflectors. For these reasons, it is desirable to observe the microwave reflection from the resonator. This is done by use of a directional coupler to feed the detector the reflected wave traveling back from the resonator.

It is proposed that a thin tube be used as a circular waveguide to transmit the microwave power from the vacuum window to the resonator and back. The waveguide used in bench tests was a 3/4 in. outside diameter SS 304 tube with a wall thickness of .020 in. The waveguide need not touch the resonator. In this way very little heat is transmitted through the waveguide. At the end of the waveguide, power is both reflected and radiated, with the radiated portion illuminating a coupling iris in the resonator mirror. The geometry is shown in Figure 22. The reflected wave contains dips at the resonance frequencies. By varying the iris geometry and the distance from the waveguide end, one can optimize Q values for the dips.

The loaded Q of the resonator is determined by:

$$Q = \frac{\omega}{\Delta\omega} \qquad (45)$$

where $\Delta\omega$ is the width of the dip between its "one-half power" point.

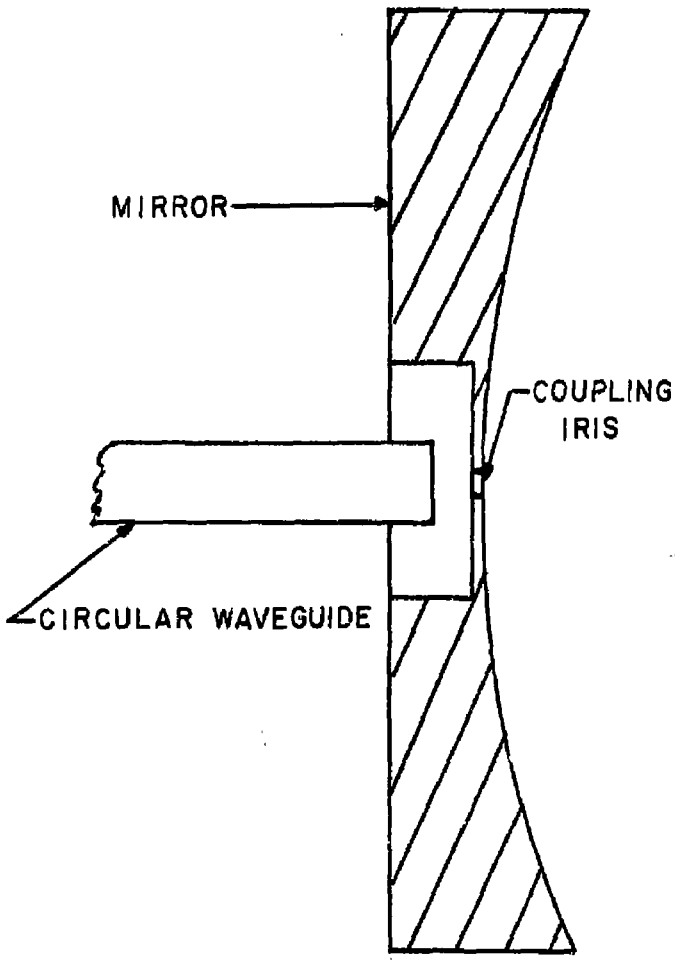

Fig. 22 Waveguide Iris Coupling to the Fabry-Perot Resonator

Measurements were made of the Q values of several resonance dips as the coupling iris size and the distance of the waveguide from the iris were varied. Several general observations can be made which are consistent with the expected behavior:

1. For larger coupling holes, the coupling is tighter and the Q's are smaller.

2. The distance of the waveguide from the iris does not greatly affect the Q, but does affect the amount of power reflected back into the waveguide.

3. For small coupling holes, the higher frequencies of the band couple much tighter than do the lower frequencies.

4. If the coupling hole size is increased, critical coupling can be exceeded and the resonance dip changes to a peak. This is shown by the resonances in Figure 23.

5. The Q of a peak is in general a factor of two to three smaller than that of a dip.

6. The coupling is relatively insensitive to mechanical vibrations in the waveguide structure.

A compromise for the overall band involved making the coupling iris small enough to keep from getting resonant peaks at the upper end of the band, but large enough to obtain enough coupling to observe significant resonant dips at the lower end of the band. For K band (18.0 GHz to 26.5 GHz) a coupling hole size of 3/16 in. in the reflector where it is only .010 in. thick, and with the waveguide 1/2 in. from the iris appeared to give the best spectrum of resonance dips. Examples of this are shown in Figure 24. Typical Q values for

the dips with this coupling range from 10,000 to 20,000 with a 1 in. by 14 in. strip of "Eccosorb AN-73" glued to the surface of the one reflector to represent the slot which is yet to be machined in it.

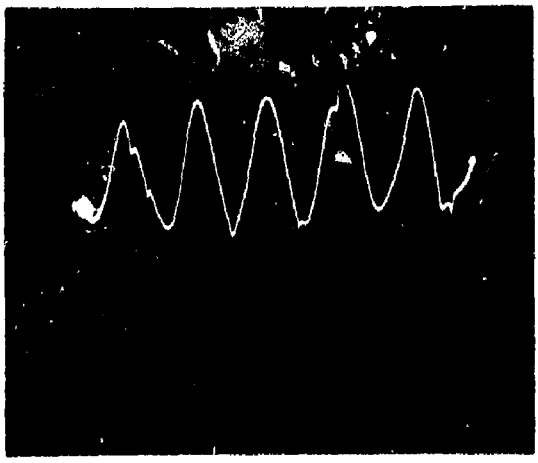

WEAK COUPLING

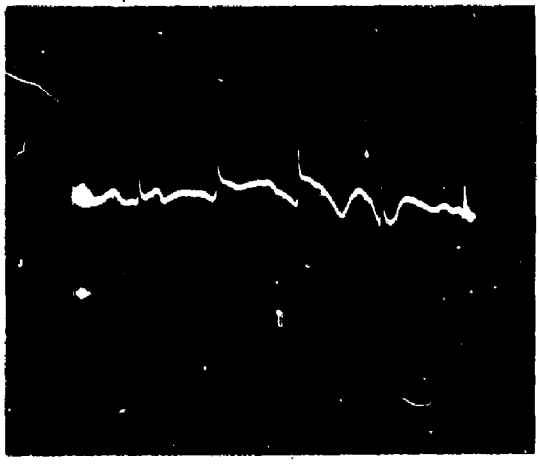

TIGHT COUPLING

Fig. 23 Resonator Resonances for Weak and Tight Coupling
(The large sinusoidal variations in the upper photo result from reflections from the back of the near reflector.)

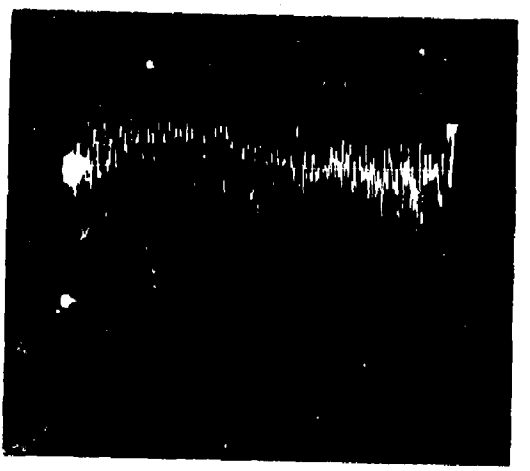

18 GHz TO 26.5 GHz

UPPER END OF BAND

Fig. 24 Resonance Dips for 3/16" Coupling Iris with the Waveguide Placed 3/4" from the Iris

VI. DISCUSSION

Evidence that spatial electron density distributions can be obtained by measuring frequency shifts of the Fabry-Perot resonator near the electron cyclotron resonance is given in this chapter. Results of the previous chapters are analyzed and recommendations are given for setting up the experiment.

ANALYSIS OF RESULTS

This section discusses the usefulness of the frequency shift data, showing that meaningful density distributions appear attainable. Difficulties in applying the theory to the reduction of data are also discussed.

Frequency Shift Data

Several criteria can be used for determining the ability of the Fabry-Perot resonator to measure a resonant frequency shift. For a Q of 10,000, and assuming that one can detect a frequency change equal to one-fifth of the half-width of a resonance peak, one could detect a frequency shift as small as .4 MHz at 20 GHz. Gardner[29] reported measurable frequency shifts of $\Delta\omega/\omega = 10^{-5}$ using a commercial signal generator without special stabilization. This implies that one could expect to measure a frequency shift as small as .2 MHz at 20 GHz. For a triangular distribution with 3×10^9 electrons/cm^3 peak, the frequency shift at 18 GHz is 2 MHz for the electron cyclotron frequency of 26.5 GHz at $z = 0$ (see Figure 10). Above 25 GHz the frequency shift is greater than 10 MHz. It thus appears that measurable frequency shifts

are readily obtainable with fair precision.

Perhaps a more useful analysis is to examine the magnitude of the differences of the frequency shifts due to plasmas with the same electron line densities but with different spatial density distributions. This would show how sensitive the resonator is to spatial variations in the density distribution. This is done for two triangular distributions having the same line densities; one having a density of 3×10^9 electrons/cm^3 at the center and going to zero at $z = \pm 14.5$ cm whereas the other has a density of 1.5×10^9 electrons/cm^3 and goes to zero at 29 cm. The lower line on the graph in Figure 10 represents the difference between the frequency shifts of these two distributions. At 18 GHz the difference is .3 MHz, at 23 GHz it is 1 MHz, and at 26 GHz the difference is 8 MHz. Clearly these frequency shifts are readily measurable, and at least the coarse features of the axial plasma distribution should be discernable by the proposed measured.

Data Reduction

There are several areas where care needs to be taken in data reduction. One of these is in determining the value of the inverse of the k by k matrix F in Equation (16). If the number of step intervals in k is large, then the elements f_{ij} have values very similar to each other, and greater precision is needed to determine the inverse when using a difference method.

The discussion in Chapter II neglected the fact that a slit 1 in. by 14 in. will be made in one of the reflectors, which will cause larger diffraction losses in the microwave field than shown by the previous analysis. Boyd and Kogelnik[30] discuss the same problem for the E field of rectangular mirrors, and determine the E field on the surface

of the mirror in closed form for the approximation of a large slit. In order to calculate the field throughout the resonator, one would still need to extend this result to the E field at an arbitrary plane between the mirrors. One might also experimentally probe the field with a dielectric material to determine the extent of the deformation. This could then be considered as a correction to the field as expressed by equation (31).

Care must also be taken in evaluating the function $f(\omega, z)$ as expressed in equation (13a). Since the electric field sensitivity to the n_e varies as E^2 where E^2 varies approximately as the cosine squared, it is necessary to take an average value of the electric field over the interval Δz. This might be done by noting that the average value of the cosine squared term is one-half, which would not be a bad approximation considering the averaging effects of the plasma. It should also be noted that the resulting integral from equation (13a) could easily be evaluated in closed form, thus greatly simplifying the computer calculation of $f(\omega_i, z_j)$.

By determining each f_{ij}, one obtains the matrix F in equation (16). The matrix N, and hence the density, is given by equation (17). One could determine the inverse F^{-1} prior to measuring frequency shifts and save this on magnetic tape, paper tape, or even in the memory core of the computer. Thus, determination of the density would be the relatively simple and fast computer operation of matrix multiplication. In this way, data could be quickly reduced, enabling perhaps time studies of the density distribution, assuming the frequency shifts could be measured fast enough.

RECOMMENDATIONS

Several recommendations can be made concerning the obtaining of data from the Fabry-Perot resonator as applied to the "Baseball II". What is needed is a method of easily determining the frequency shifts for each polarization, and a method to record the data so that it is easily recovered and reduced.

Methods to clean up the swept frequency spectrum of the reflection from the Fabry-Perot resonator might include designing an RC high-pass filter to filter out the slowly varying AC component and yet retain the sharp resonance dips, if the frequencies are swept sufficiently fast. Further work with coupling to reduce the reflection from the backside of the resonator might also be tried. In calibrating the frequency shift magnitudes a separate and identical cavity might be operated outside the vacuum container to establish reference points. The two cavities could be tuned to each other before the plasma is turned on.

It has also been suggested that the analog magnetic tape system presently used with the "Baseball II" system might easily be adapted to record the reflected signal and a reference signal as a function of the time. It would thereby be possible to make many runs and analyze the time dependence of the density distribution. One could analyze the tape leisurely after the runs, perhaps with the PDP-8 system in use with the experiment. This tape system is capable of recording twelve inputs simultaneously.

The discussion here has been in terms of the right-hand circular polarization modes only. If one excites the resonator by a linear polarized wave, degeneracy is removed with each polarization

shifting in frequency by a different amount. One could simplify the resulting spectrum of peaks by using a filter which transmits only one circular polarization. A turnstile junction might be used in this application in spite of its narrow bandwidth. However, with appropriate designing of the junction the bandwidth may be made broad enough to observe sufficient resonances to permit the calculation of density distributions.

VII. SUMMARY

The aim of this thesis is to theoretically study the application of a microwave Fabry-Perot resonator in a minimum-B plasma to obtain spatial electron density distributions, and also to build and test a circular tunable microwave vacuum window to allow diagnosis with circular polarization and to determine a means to couple power to and from the Fabry-Perot resonator. The problem is discussed in terms of the "Baseball II" experiment at the Lawrence Livermore Laboratory of the University of California, the objective being to study the feasibility of using this technique on the "Baseball II" plasma experiment.

The method is based on the behavior of the dielectric constant of a plasma as the operating frequency approaches the electron cyclotron frequency. The frequencies of the Fabry-Perot resonator are thus changed by addition of a plasma in a manner that depends on the spatial characteristics of the magnetic field. In a low β plasma, the spatial variation of the magnetic field strength is known, allowing one to calculate a spatial sensitivity function for frequency shifts of the resonator. By allowing the axial electron density distribution of the plasma to be approximated by a stepped function, one is able to work backwards from the frequency shifts of several resonances to obtain the density distribution.

The results of the theory are not tested in this thesis since this would need to be done with the actual plasma. Several

approximations are made, and the expected frequency shifts are determined for various assumed electron density distributions. A plot of the spatial sensitivity versus axial position is also given.

A tunable microwave window device was built in circular waveguide utilizing two dielectric disks as vacuum windows separated one quarter of the guide wavelength from each other, and was tested from 18 to 26.5 GHz by a swept-frequency VSWR technique. The tests of the window showed a wide-band response, and that the window tuned to the central part of the band has a VSWR of 1.1 and less than 2.2 at the extremes.

The Q values of the resonator determined for optimal coupling varied from 10,000 to 20,000 across the band, with a one inch slot in one of the mirrors.

The frequency shift plots show that for a peak density in the center of 3×10^9 electrons/cm^3 and the electron cyclotron frequency at 26.5 GHz at the center, the expected frequency shift is 2 MHz at 18 GHz and above 10 MHz above 25 GHz. The plot of the spatial sensitivity also shows that the frequency shift is greatly varied by varying the plasma location and microwave frequency.

The use of the Fabry-Perot interferometer utilizing the spatial variation of the static confining magnetic field promises to be capable of yielding spatial electron density distributions along the z axis. Two experimental problems, that of building a vacuum window to allow transmission of circular polarizations, and that of determining a method of coupling, have been solved. The application of this experimental technique to the "Baseball II" experiment is recommended.

LIST OF REFERENCES

1. William C. Gough and Bernard J. Eastlund, "The Prospects of Fusion Power," Scientific American 224, 50 (1971).

2. M. A. Heald and C. B. Wharton, Plasma Diagnostics with Microwaves, (John Wiley and Sons, Inc., New York, 1965), p. 366.

3. Roger J. Chaffin, "Application of the Microwave Fabry-Perot Resonator to Plasma Diagnostics" (unpublished Doctor's dissertation, University of Wisconsin, 1967), p. 27.

4. Roger J. Chaffin, "Application of the Microwave Fabry-Perot Resonator to Plasma Diagnostics" (unpublished Doctor's dissertation, University of Wisconsin, 1967), p. 14.

5. G. D. Boyd and J. P. Gordon, "Confocal Multimode Resonator for Millimeter through Optical Wavelength Masers," Bell System Tech. J. 40, 489 (1961).

6. G. D. Boyd and H. Kogelnik, "Generalized Confocal Resonator Theory," Bell System Tech. J. 41, 1347 (1962).

7. G. Goubau and F. Schwering, "On the Guided Propagation of Electromagnetic Wave Beams," IRE Trans. Antennas and Propagation AP-9, 248 (1961).

8. R. I. Primich and R. A. Hayami, "The Application of the Focussed Fabry-Perot Resonator to Plasma Diagnostics," IEEE Trans. Microwave Theory and Techniques MTT-12, 33 (1964).

9. Roger J. Chaffin and James B. Beyer, "Diagnostics of an Anisotropic Plasma with a Microwave Fabry-Perot Resonator," IEEE Trans. Microwave Theory and Techniques MTT-16, 878 (1968).

10. Roger J. Chaffin and James B. Beyer, "Plasma Diagnostics with a Microwave Fabry-Perot Resonator," IEEE Trans. Microwave Theory and Techniques MTT-16, 37 (1968).

11. K. E. Lonngren, J. W. Mink and J. B. Beyer, "On the Focused Fabry-Perot Resonator in Plasma Diagnostics," IEE Trans. Microwave Theory and Techniques MTT-12, 548 (1964).

12. S. R. Seshadri, "Plasma Diagnostics with a Fabry-Perot Resonator," Proc. IEEE 57, 1187 (1969).

13. D. E. McCumber, "Eigenmodes of a Symmetric Cylindrical Confocal Laser Resonator and their Perturbation by Output-Coupling Apertures," Bell System Tech. J. 44, 333 (1965).

14. Robert W. Zimmerer, "Spherical Mirror Fabry-Perot Resonators," IEEE Trans. Microwave Theory and Techniques MTT-11, 371 (1963).

15. Lev Albertovich Weinstein (Vaynshteyn), Open Resonators and Open Waveguides (The Golem Press, Boulder, Colorado, 1969), p. 112.

16. Herwig Kogelnik, In Lasers, Edited by Albert K. Levine, (Marcel Dekker, Inc., New York, 1966), p. 295.

17. H. K. V. Lotsch, "The Fabry-Perot Resonator," Optik 28, 338 (1968).

18. Reuben Eaves, Thomas G. Twardeck and Stephen J. Moren, "Determination of Plasma Electron-Density Distribution from the Resonant Frequencies of a Parallel-Plate Cavity," IEEE Trans, Antennas and Propagation AP-19, 221 (1971).

19. A. L. Gardner, "A Proposed Microwave Technique to Measure Spatial Electron Distribution of Electron Density," Bull. Am. Phys. Soc. 16, 1237 (1971).

20. From personal correspondence between Dr. James Foote of Lawrence Livermore Laboratory, University of California, and Dr. A. L. Gardner, Physics Department, Brigham Young University.

21. Roger F. Harrington, Time Harmonic Electromagnetic Fields, (McGraw-Hill Book Company, Inc., New York, 1961), p. 317-365.

22. Roger J. Chaffin, "Application of the Microwave Fabry-Perot Resonator to Plasma Diagnostics" (unpublished Doctor's dissertation, University of Wisconsin, 1967), p. 135.

23. M. A. Heald and C. B. Wharton, Plasma Diagnostics with Microwaves, (John Wiley and Sons Inc., New York, 1965), pp. 15, 32.

24. M. P. Bachynski and B. W. Gibbs, "Propagation in Plasmas along the Magnetic Field," Phys. Fluids 9, 520 (1966).

25. William P. Allis, Solomon J. Buchsbaum and Abraham Bers, Waves in Anisotropic Plasmas, (M.I.T. Press, Cambridge, Massachusetts, 1963), p. 21.

26. IBM Application Guide, System/360 Scientific Subroutine Package, Version III Programmers Manual, (IBM, White Plains, New York, 1968).

27. H. Kogelnik and T. Li, Appl. Opt. 5, 1560 (1966).

28. G. D. Boyd and J. P. Gordon, "Confocal Multimode Resonator for Millimeter through Optical Wavelength Masers," Bell System Tech. J. 40, 499 (1961).

29. A. L. Gardner, "Detection of the Shift of Resonant Frequencies of an Array of Microwave Cavities," Bull. Am. Phys. Soc. 13, 275 (1968).

30. G. D. Boyd and H. Kogelnik, "Generalized Confocal Resonator Theory," Bell System Tech. J. 41, 1357 (1962).

APPENDIXES

APPENDIX A

VACUUM WINDOW DRAWINGS

In Figures 25 through 30 detailed drawings of the vacuum window are given. Figure 13 shows all of these parts assembled.

All parts are brass except the vacuum flange in Figure 25, which is stainless steel 304.

The vacuum flange is designed to conform with the flanges of the "Baseball II".

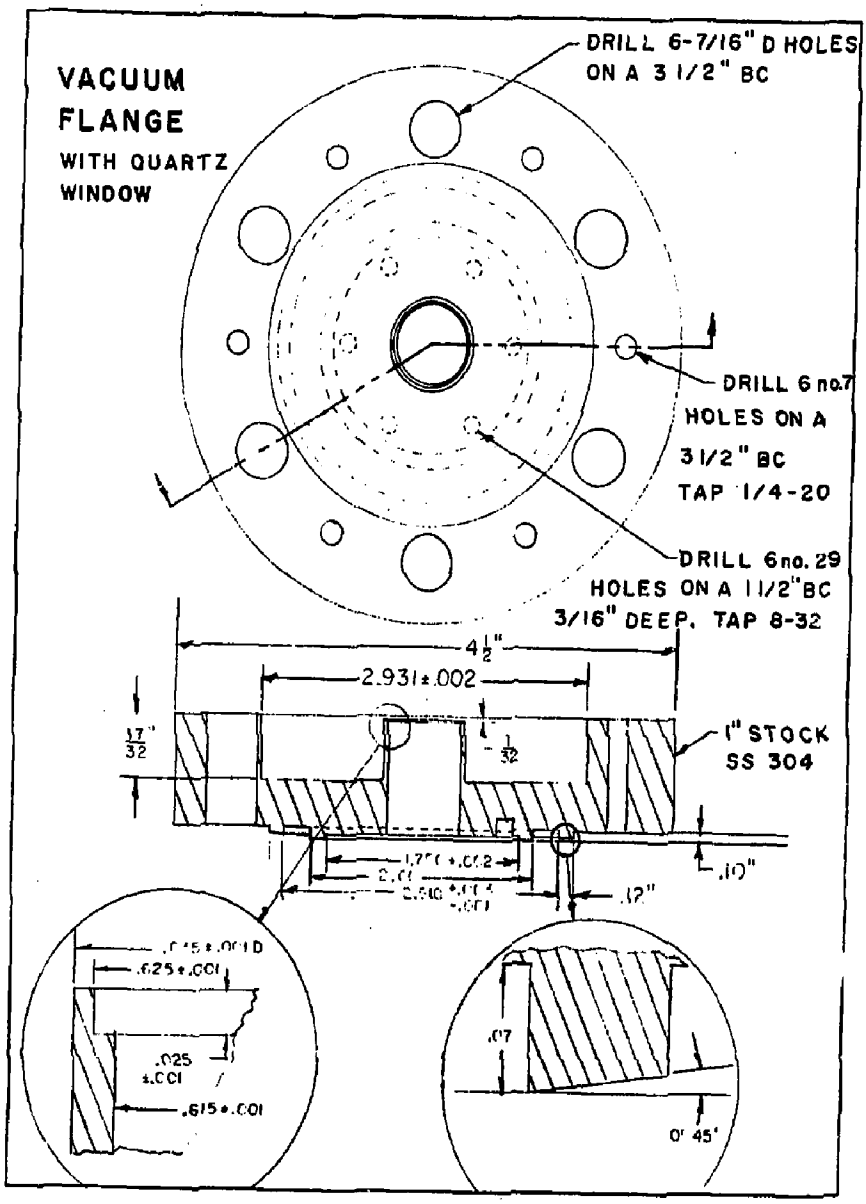

Fig. 25 The Vacuum Flange

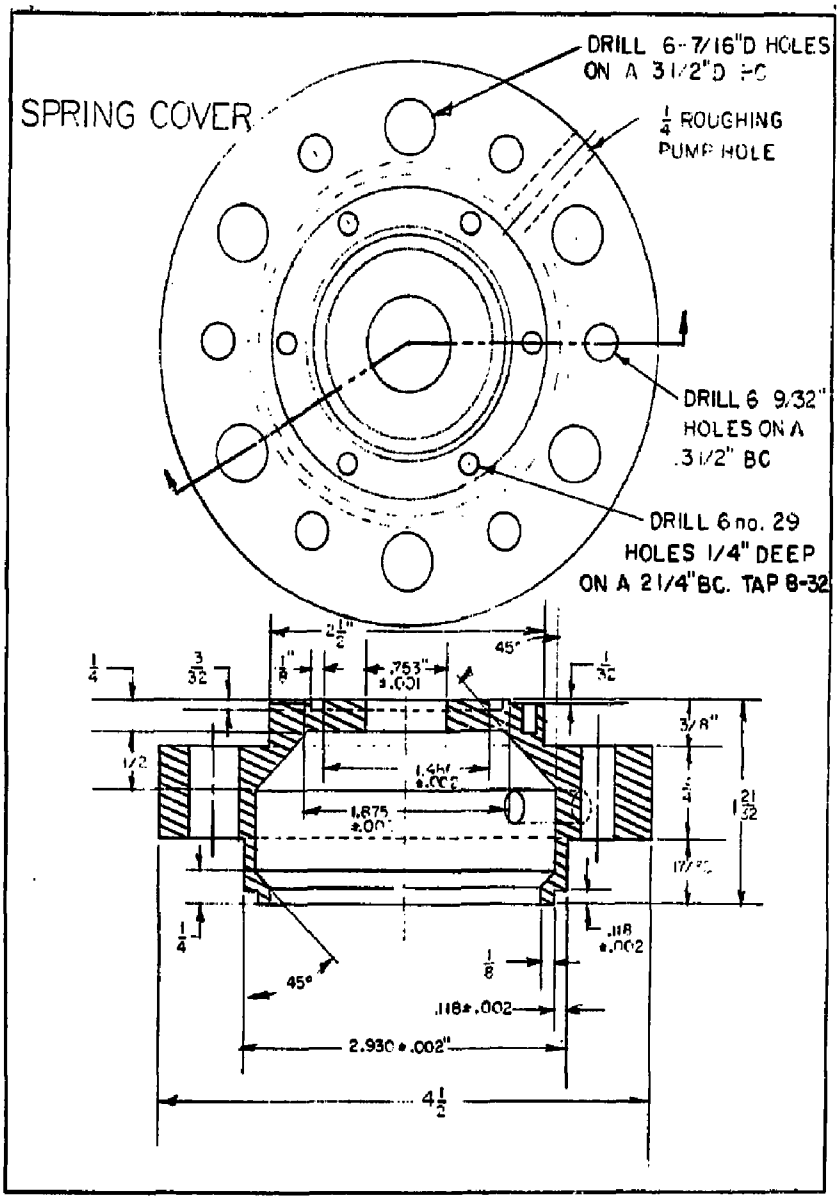

Fig. 26 Spring Cover

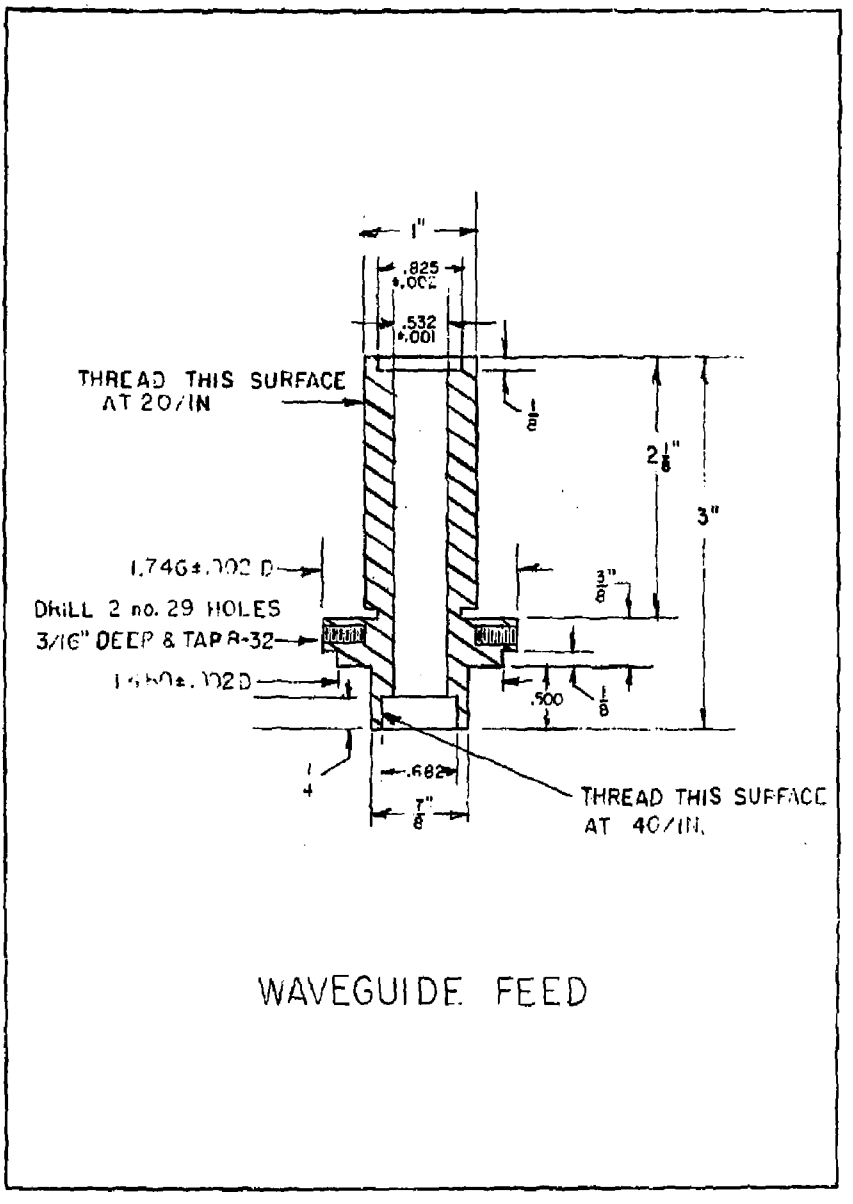

Fig. 27 Waveguide Feed

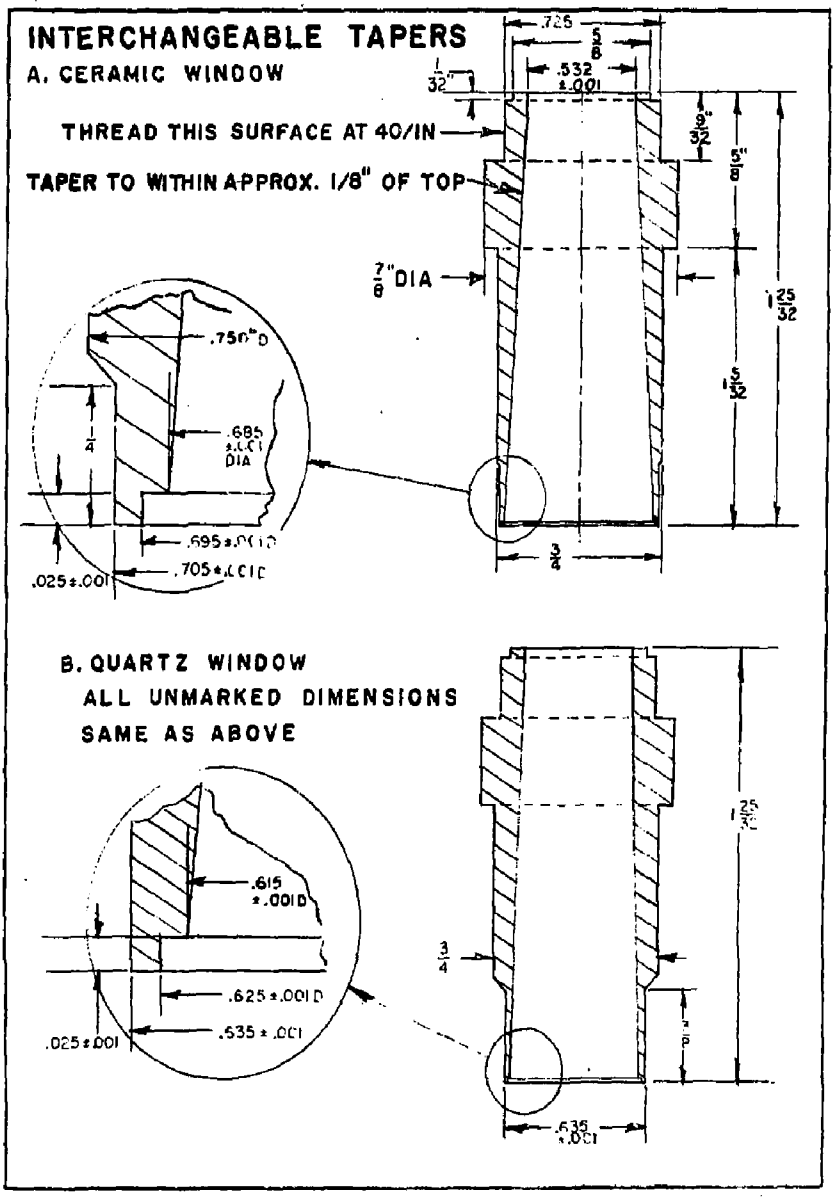

Fig. 28 Interchangeable Tapered Waveguide Sections

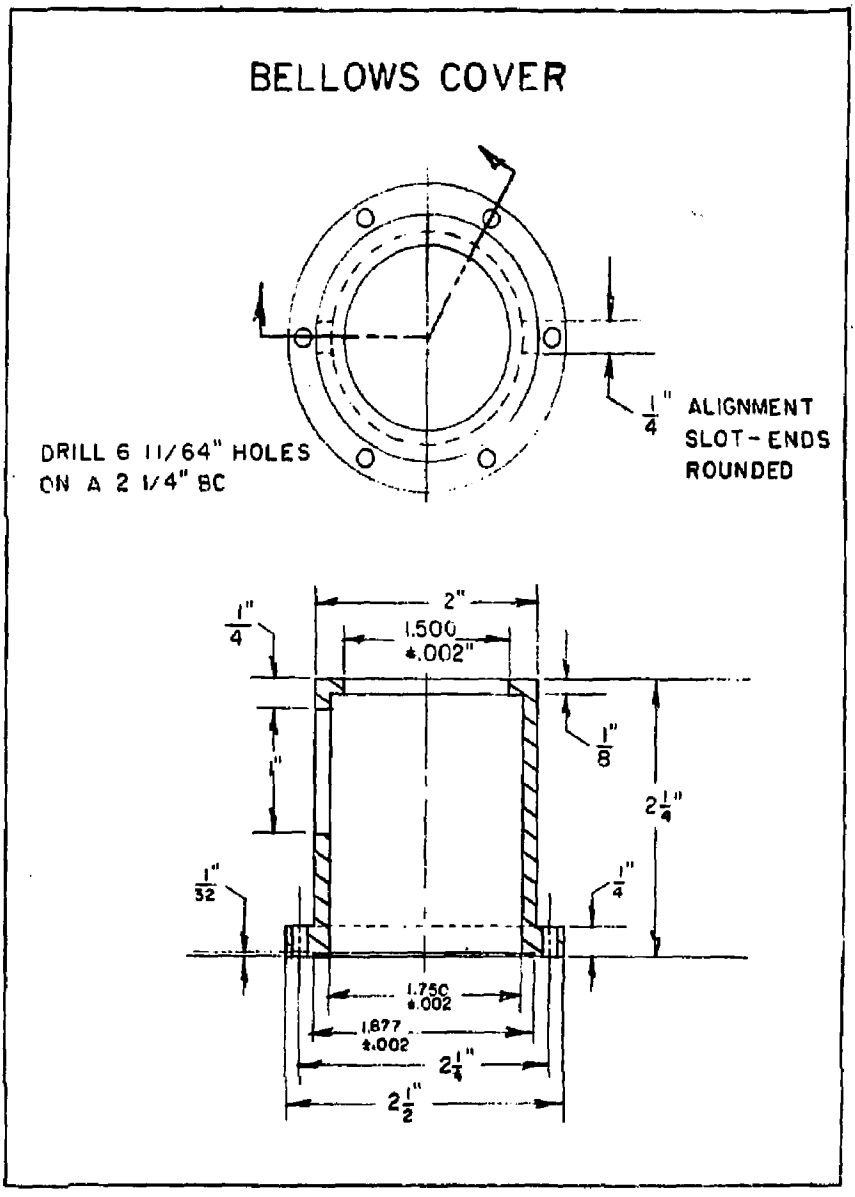

Fig. 29 Bellows Cover

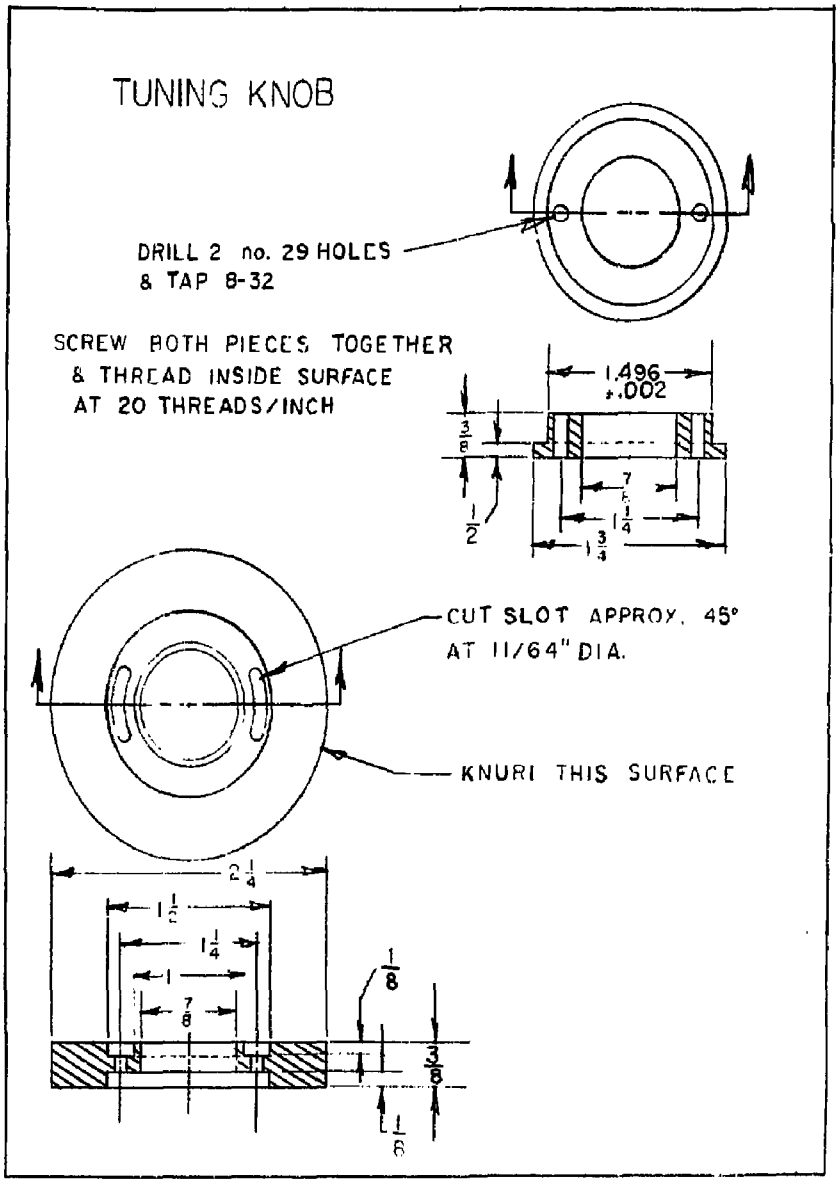

Fig. 30 Tuning Knob

APPENDIX B

PHOTOGRAPHS OF THE VACUUM WINDOW STANDING WAVE PATTERNS

The tunability of the vacuum window is easily observed by looking at the standing wave pattern the window generates as it is tuned to a particular frequency. Figures 31 through 36 and Figures 37 through 42 show standing wave envelopes for quartz and ceramic windows. Figure 20 shows how this data was taken. The horizontal scale is from 18.0 GHz to 26.5 GHz, and the vertical scale is the detector output from the slotted line.

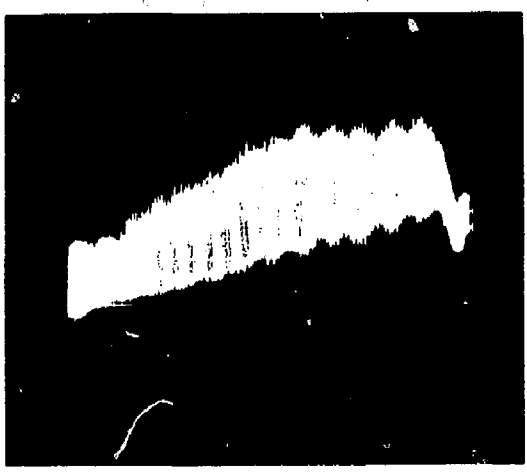

Fig. 31 Standing Wave Envelope for the Quartz Window at .50 Turns

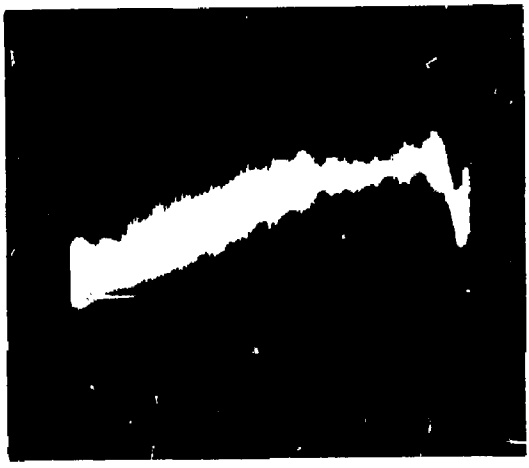

Fig. 32 Standing Wave Envelope for the Quartz Window at .90 Turns

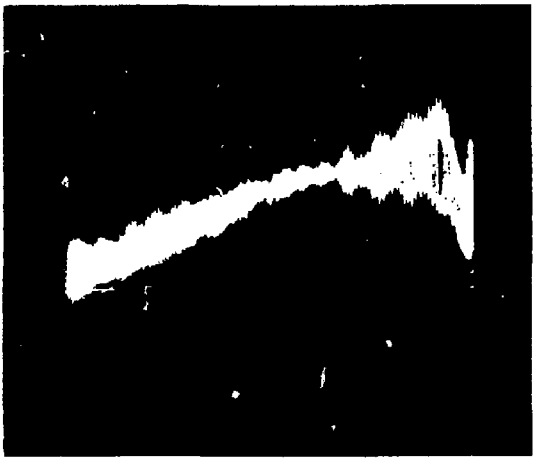

Fig. 33 Standing Wave Envelope for the Quartz Window at 1.10 Turns

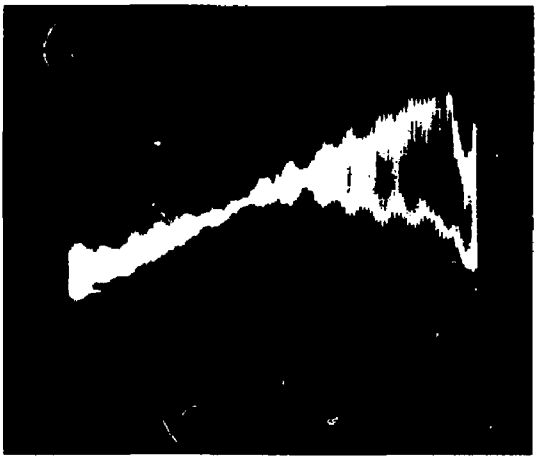

Fig. 34 Standing Wave Envelope for the Quartz Window at 1.30 Turns

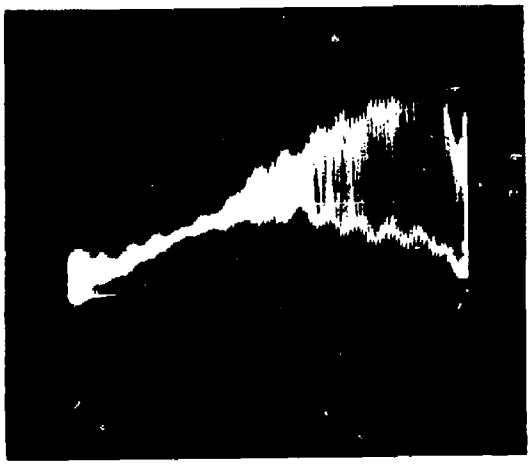

Fig. 35 Standing Wave Envelope for the Quartz Window at 1.50 Turns

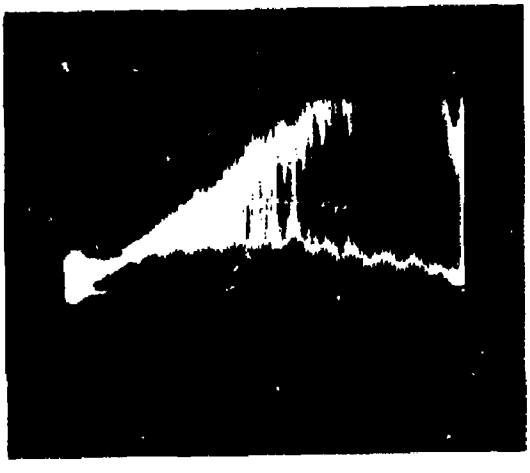

Fig. 36 Standing Wave Envelope for the Quartz Window at 1.90 Turns

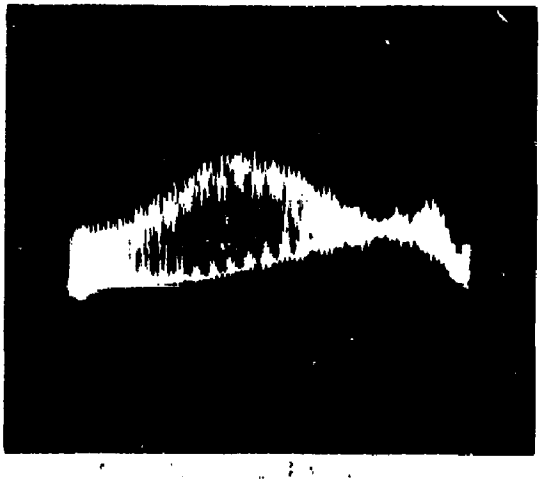

Fig. 37 Standing Wave Envelope for the Ceramic Window at -0.10 Turns

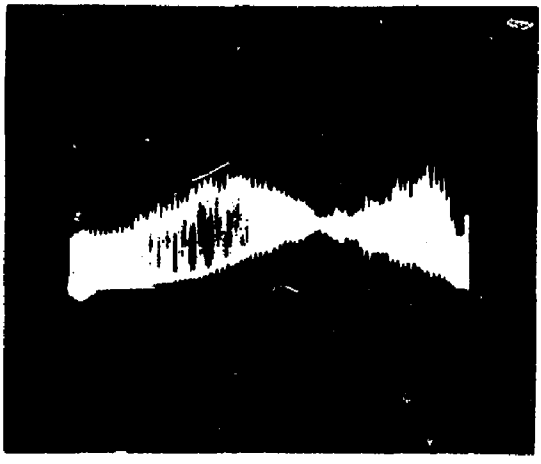

Fig. 38 Standing Wave Envelope for the Ceramic Window at 0.00 Turns

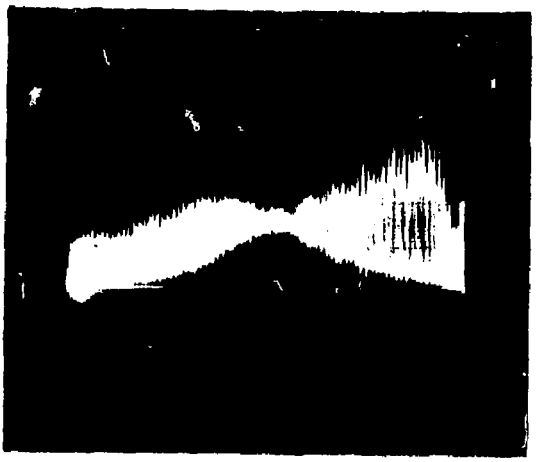

Fig. 39 Standing Wave Envelope for the Ceramic Window at 0.10 Turns

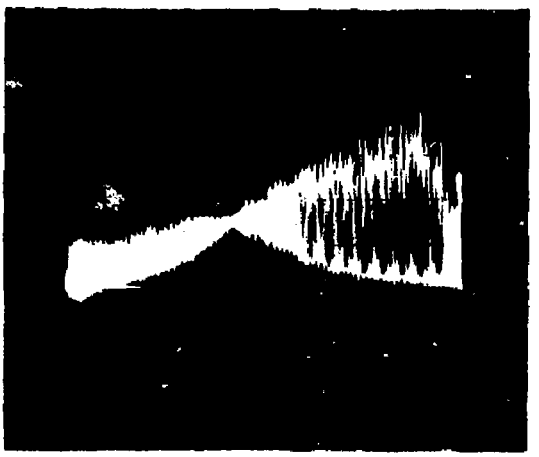

Fig. 40 Standing Wave Envelope for the Ceramic Window at 0.20 Turns

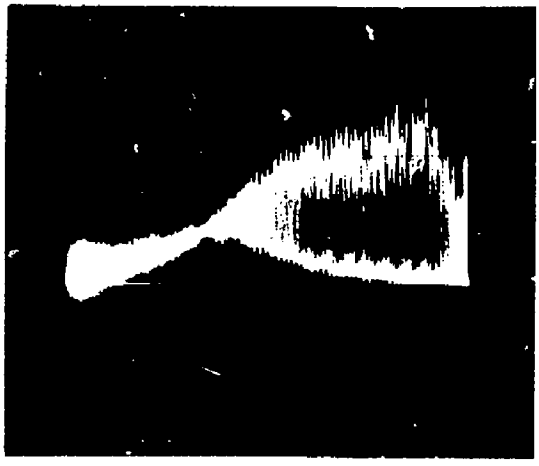

Fig. 41 Standing Wave Envelope for the Ceramic Window at 0.30 Turns

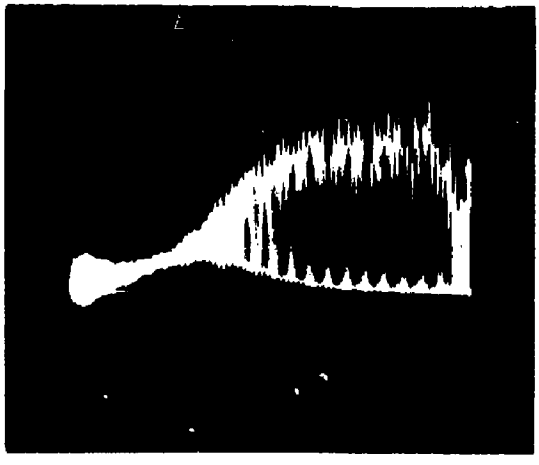

Fig. 42 Standing Wave Envelope for the Ceramic Window at 0.40 Turns

APPENDIX C

FREQUENCY DEPENDENCE OF THE VSWR

The VSWR was calculated from a standing wave smear envelope plot from an x-y recorder for various settings of the quartz vacuum window tuning mechanism. These are shown in Figures 43 through 47.

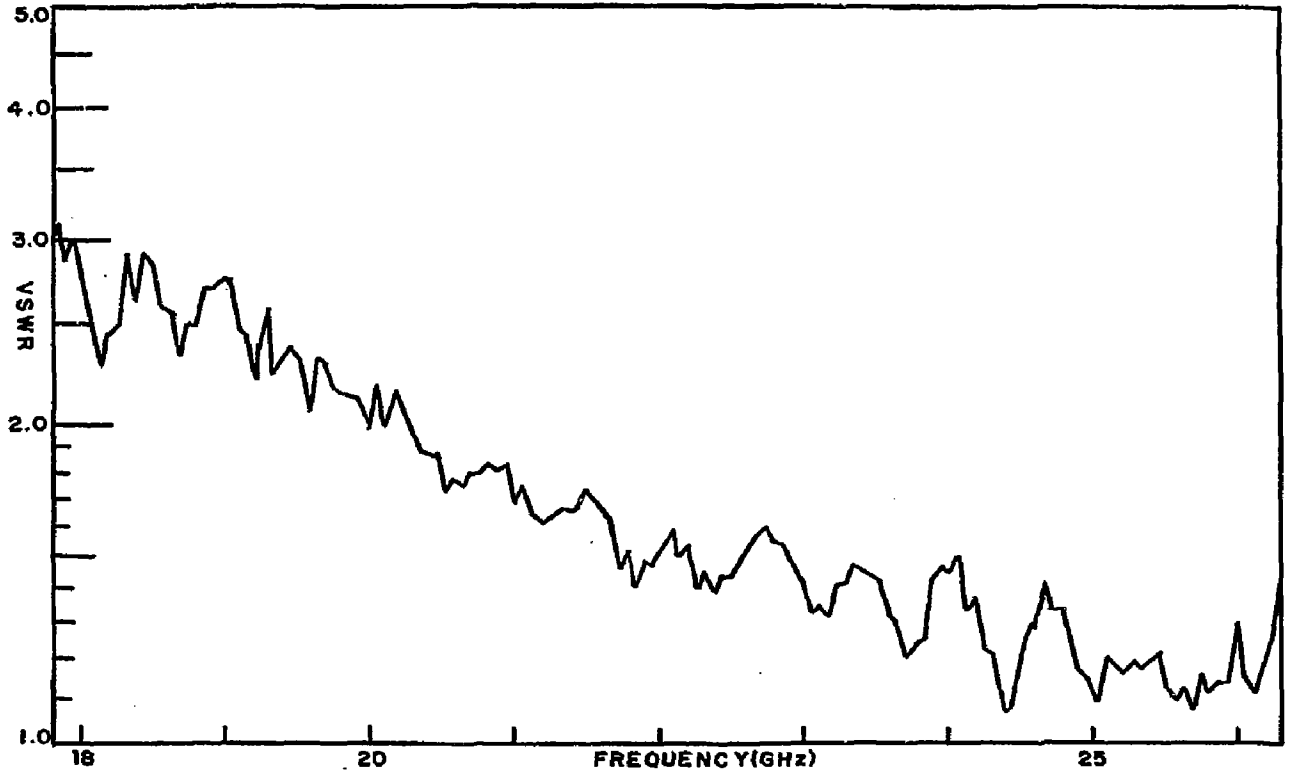

Fig. 43 Frequency Dependence of the VSWR for the Quartz Window for 0.70 Turns

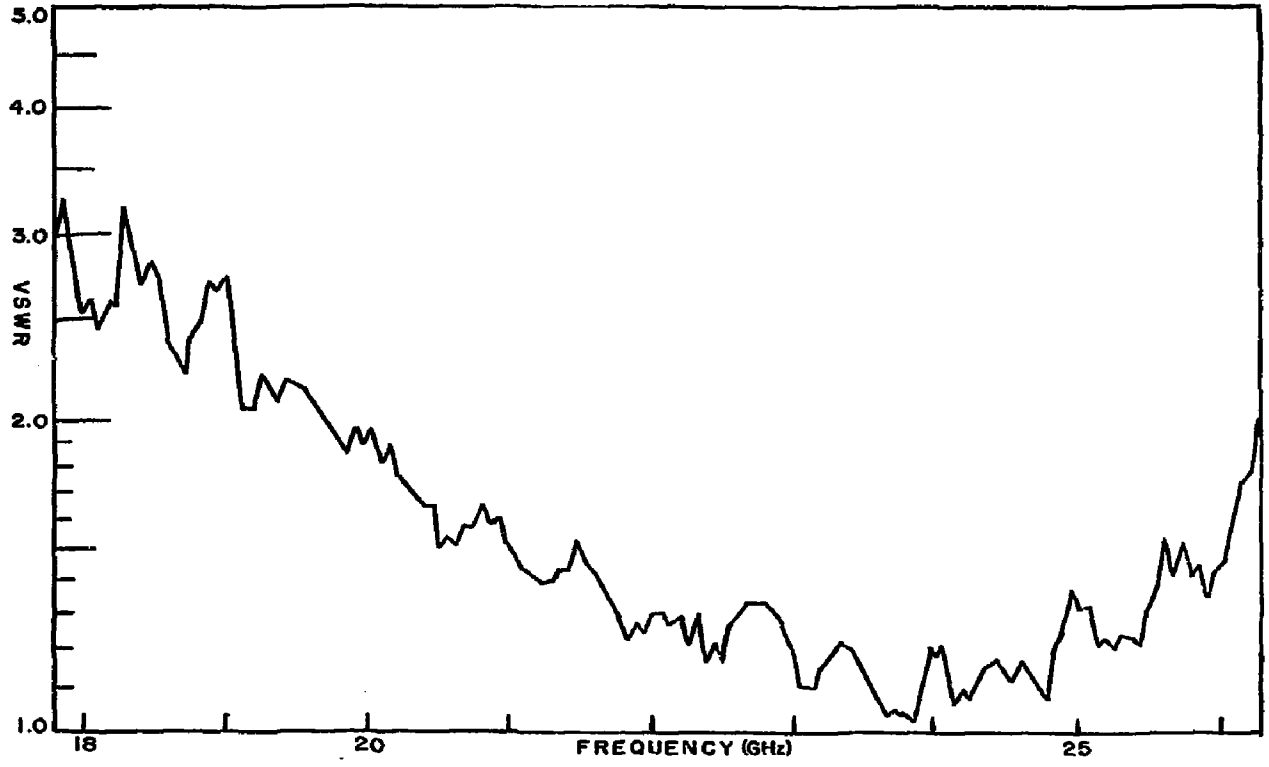

Fig. 44 Frequency Dependence of the VSWR for the Quartz Window for 0.90 Turns

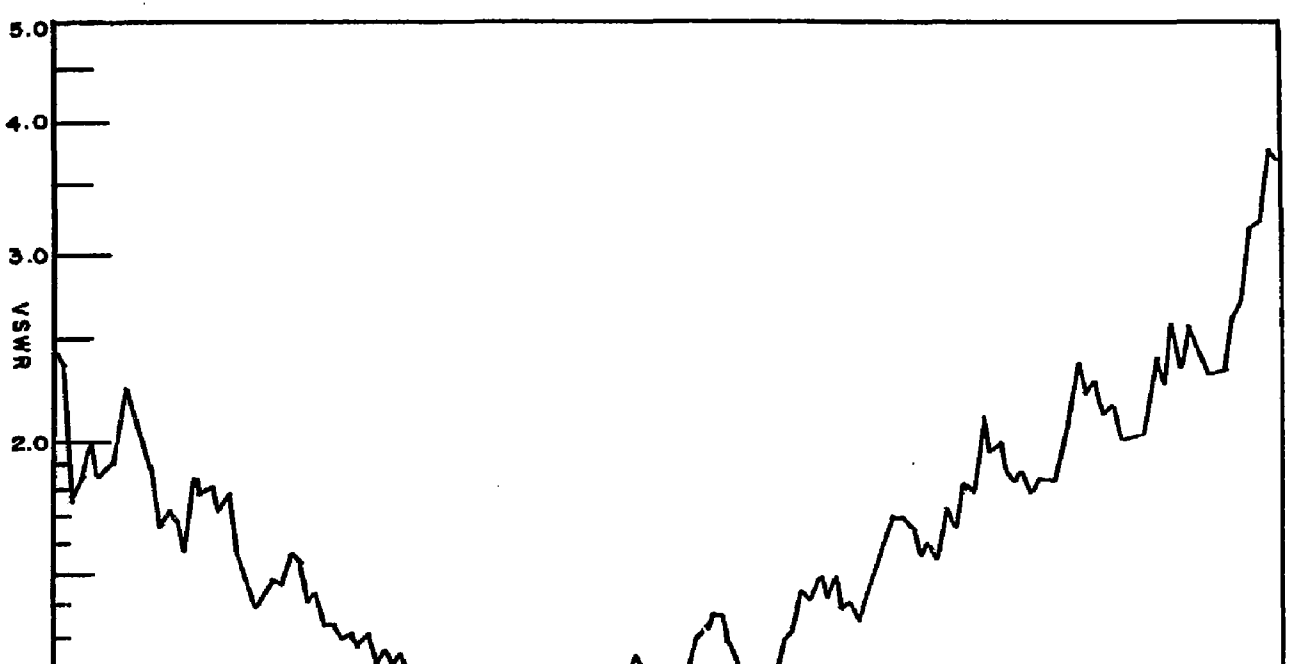

Fig. 45 Frequency Dependence of the VSWR for the Quartz Window for 1.30 Turns

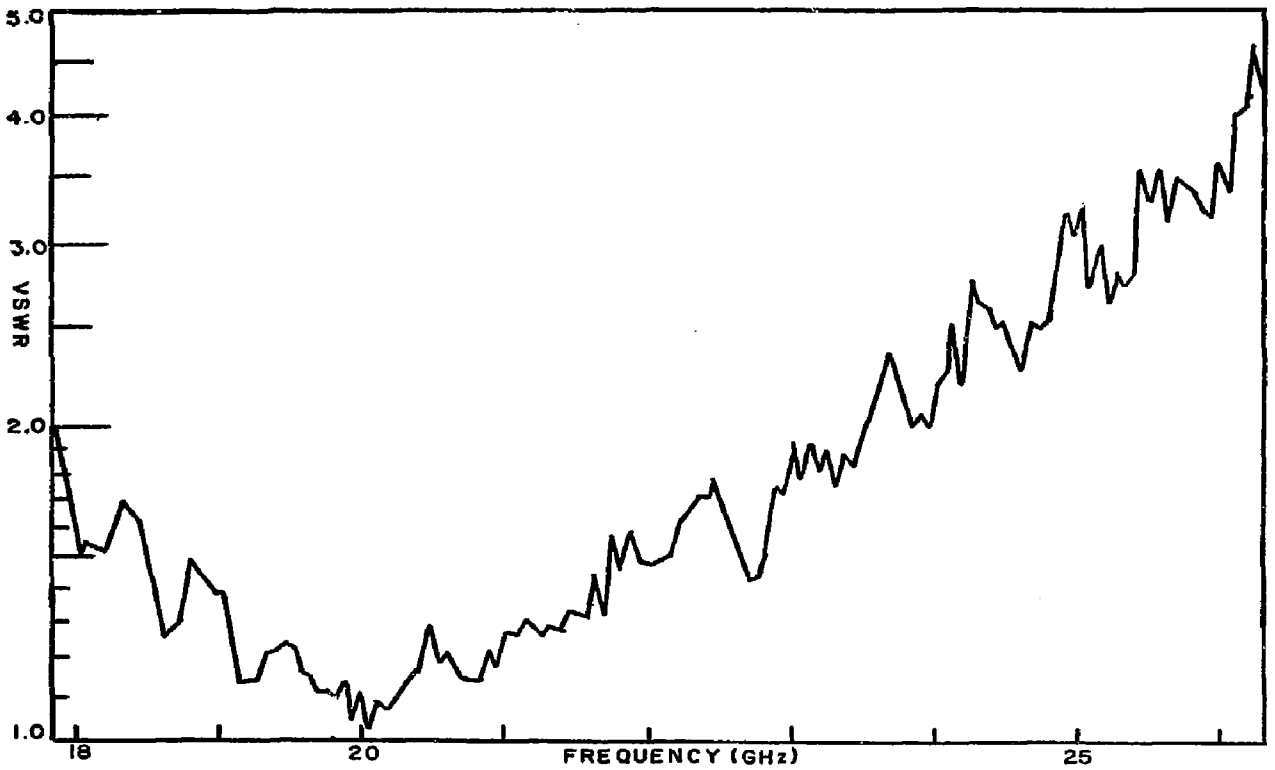

Fig. 46 Frequency Dependnece of the VSWR for the Quartz Window for 1.50 Turns

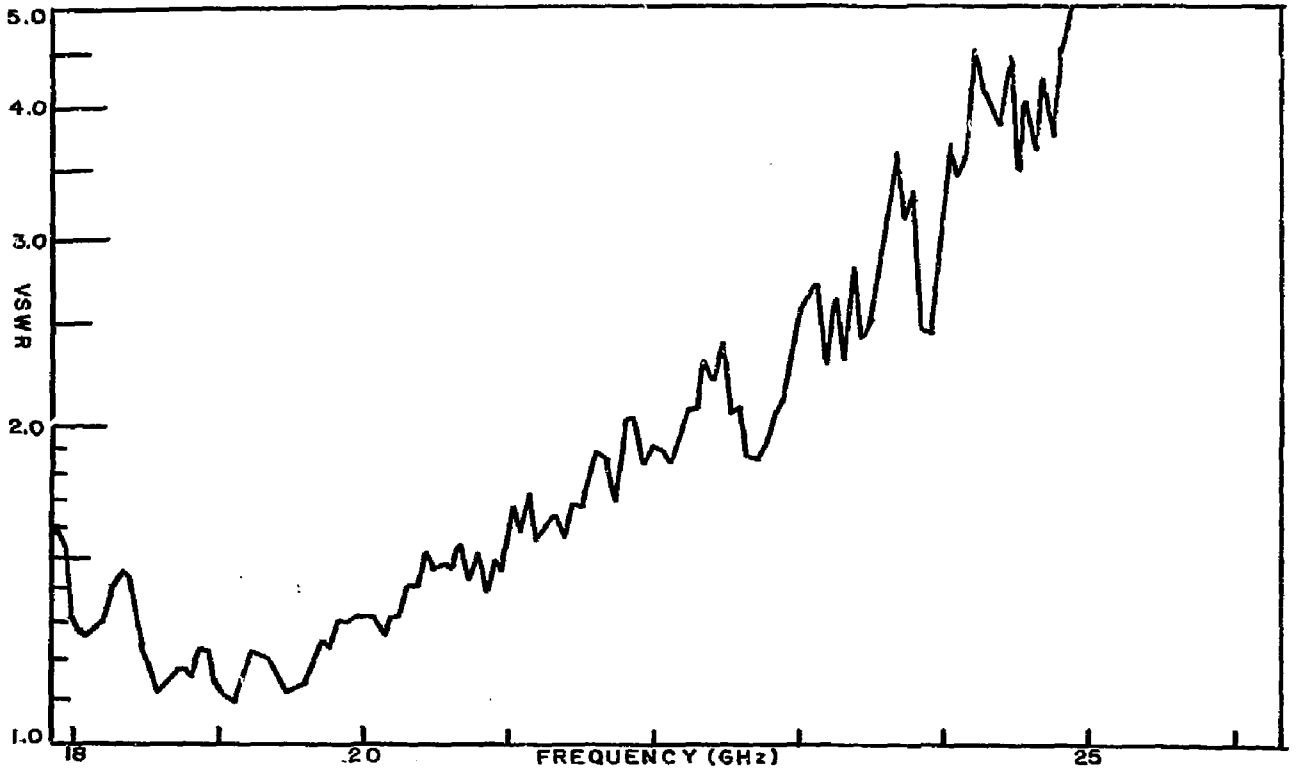

Fig. 47 Frequency Dependence of the VSWR for the Quartz Window for 1.90 Turns